AIMS Geosciences

AIMS Geosciences, 11(3): 600–628.
DOI: 10.3934/geosci.2025026
Received: 02 February 2025
Revised: 24 May 2025
Accepted: 18 June 2025
Published: 21 July 2025

https://www.aimspress.com/journal/geosciences

Research article

Engineering properties and characterisation of sediments at the Belgrade Waterfront test site

Dušan Berisavljević*and Zoran Berisavljević

Geotechnical Department, Faculty of Mining and Geology, Belgrade University, Đušina 7, Serbia

* **Correspondence:** Email: dusan.berisavljevic@rgf.bg.ac.rs; Tel: +38166106805.

Abstract: The Belgrade Waterfront (BW) is one of the largest ongoing construction sites in the Republic of Serbia. It is located at the confluence of two major rivers, the Danube and Sava, where natural soil conditions vary from soft clays, silts, and sands to heavily overconsolidated marls underlined by limestone. The geological conditions encountered on the BW site can be considered a benchmark test site for other sites in Belgrade with similar ground conditions. Various in situ tests were performed to characterize ground conditions. The most important tests used were the bi-directional pile static load test (BD test), seismic dilatometer test (SDMT), piezocone penetration test (CPT), and Menard pressuremeter test (MPT). We focused on the ground investigation performed at two plots. Plot 12 was closer to the confluence, where marl was thinner and softer compared to plot 19, where marl was thicker, with preserved microstructure, and was less influenced by water from alluvial deposits lying above. Our intention of this research was to address some of the most important factors that influence soil behavior and their significance for the interpretation of in situ tests. Those factors are partial consolidation effects (rate effect), microstructure, and stress history. Having a good understanding of geological conditions at the site, the applicability of common correlations used to derive stress history, stiffness, and strength parameters from in situ tests were assessed for various soil types. It was shown that partial consolidation around the dilatometer blade can develop in the lower parts of floodplain sediments. Marls behave undrained for standard rates of penetration and testing. However, microstructure influences the interpretation of in situ tests, particularly CPT, in terms of soil type. Following the basic CPT classification, marl is described as a coarse-grained soil. However, the CPT also indicated high measured pore pressure at the piezo element, suggesting the presence of fine-grained material. According to previous research, this behavior is common for soils with a

microstructure. It was shown that OCR in alluvial silty clay and marls can be overpredicted 3–4 times from common CPT correlations integrated in commercial software. This uncertainty may be attributed to unusual soil conditions in terms of microstructure and partial drainage effects. The interpretation of MPT results indicated that marls have distinct strain-softening behavior, while macrostrain measurements from the BD test indicate nonlinear softening of skin friction in limestone.

Keywords: microstructure; marl; over consolidated; strain softening; bi-directional pile load test

1. Introduction

As recognized by the Government of the Republic of Serbia, the Belgrade Waterfront (BW) is a monumental urban revitalization project worth US$ 3 billion. It is planned as a new city center and one of the major tourist destinations in Belgrade, located on the right bank of the Sava River close to its confluence with the Danube River. It is the second-largest mixed-use complex under construction in Europe. It was started in 2014 and is still an active construction site.

In the past decade, there has been a positive trend of establishing geotechnical experimentation sites all around the world. Geo-sites are intended for testing and verifying innovative soil investigation methods and foundation solutions [1]. Each of those sites consists of a particular soil type formed in a specific depositional environment. Some sites consist of more or less uniform deposits of clay [2–5], silt [6,7], and sand [8], while others are more heterogeneous in terms of soil type [9,10]. Currently, in Serbia, geo-experimentation sites are not established. However, recent construction activities, with large investments, made it possible to perform several high-quality geotechnical investigation campaigns, enabling a better understanding of soil behavior with respect to foundation design, stability of deep excavations, and embankment construction. Two well-explored sites that stand out are the Belgrade Waterfront (BW) and EXPO 2027 sites. Here, we focus on the BW site, where ground conditions consist of various soil types formed in different depositional environments. Younger sediments are formed by river action and consist of soft clays, silts, and sands, while older sediments, consisting of marls, are formed in the sublittoral parts of the long-lived Lake Pannon during the Late Miocene. Our aim of this paper is to show recently obtained results and to characterize soil utilizing common in situ tests for site characterization: Piezocone penetration test (CPT), seismic dilatometer test (SDMT), and Menard pressuremeter test (MPT). In addition to in situ tests, results of the bi-directional pile static load test (BD test) are shown with emphasis on load-transfer mechanisms in marls and organogenic reef limestone, which represent a bedrock for a test site. Correlations used to derive soil parameters from in situ tests, frequently encountered in the literature, are evaluated. Intercomparison of SDMT and CPT test results is shown. Particular attention is given to the determination of the microstructure in a soil using soil behavior type charts (SBT), which rely on large-strain parameters or a combination of large and small strain parameters. The BW ground conditions are typical for the Belgrade area, and their characterization is significant for the development of other parts of Belgrade. Regarding those terms, BW can be considered a benchmark test site for other sites across Belgrade.

2. A brief history of the development of the BW site

Historically, this area was called Bara Venecija (in Serbian), literally translated (in English) as Pond Venice, pointing out the similarity with the Venetian Lagoon in Italy. The old Sava bridge is founded on wooden piles, a material commonly used as a construction material in Venice. Some geotechnical aspects of the Venetian Lagoon can be found in [10]. Figure 1 compares an aerial view of Bara Venecija from 1934 and a modern view of BW at its current state of development. Bara Venecija is known to be a rural part of Belgrade where its development is mostly related to the construction of a railway connecting Serbia with Austro-Hungary [11]. The construction of the railway started in 1878, and it was opened for traffic in 1884. The railway construction activities are important in terms of site development since most of the area covered with ponds was filled with material from local excavations and even from parts of the demolished Kalemegdan fortress made by the Turks during their occupation of Belgrade. Another important event that influenced the hydrology regime of Belgrade is the construction of the Hydroelectric Power Station Djerdap (HPS), located at the Serbian-Romanian border, 227 km from Belgrade. The construction of HPS Djerdap has led to changes in the water regime of the Danube River and its tributaries. Due to backwaters formed by the construction of HPS Djerdap, the Sava River, as the most important tributary of the Danube, rose approximately 2 m in Belgrade. This raise influenced the regime of underground water in Belgrade, particularly the riverbank area, creating the need for additional landfilling to raise elevation at Bara Venecija [12].

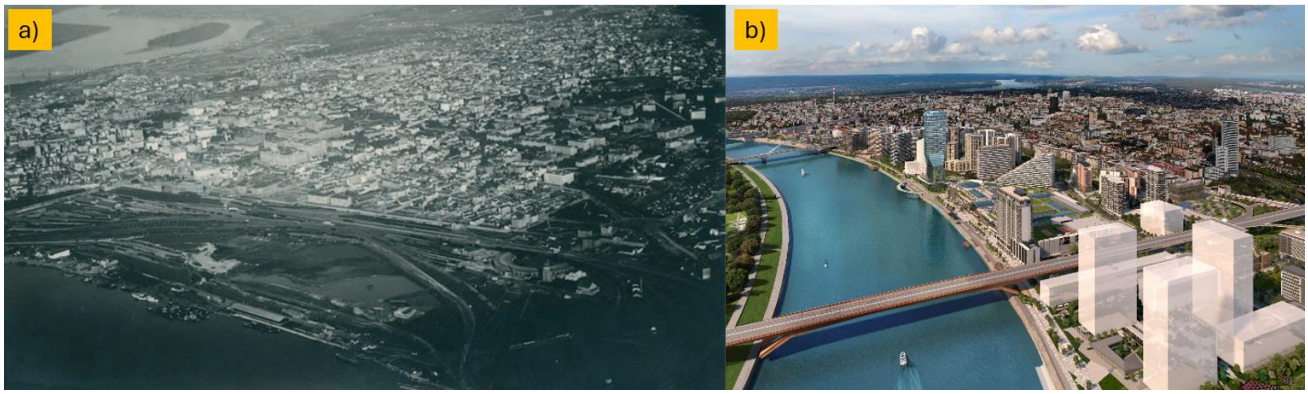

Figure 1. Aerial view of Bara Venecija (BW): a) Aerial view taken in 1934, and b) digital model at the current state of construction.

BW's key icon at the centre of the waterfront is Tower Belgrade, Serbia's tallest tower with a height of 168 m. High-rise buildings impose large loads on the foundation, and given thick layers of soft soils below the foundation level, all buildings are designed on pile foundations. Deep excavations for underground floor construction pose one of the major construction challenges. At some locations, the excavation depth is ten meters or more below the average annual water level of the Sava River; thus, to establish dry construction and lower water pressures, a system of wells and observation objects had to be made and put into operation. Most of the design issues are related to ground conditions whose engineering properties have to be reliably evaluated.

3. Site description

The BW site consists of 40 plots covering a total area of 177 ha. The master plan of the site is shown in Figure 2. We focused on plot 12 and central plot 19, on which Tower Belgrade was built. Plot 12 is chosen given that parallel CPT and SDMT soundings were performed, which allowed comparison of parameters measured by these tests. On plot 19, for the first time in the Balkan region, Osterberg load cells were used to perform a BD static pile load test. Measuring the unit shaft friction and end bearing from static load tests is not a common practice in Serbia, which highlights the importance of experience gained from BD tests. The tower was constructed on 37 m long drilled piles resting on the bedrock composed of organogenic reef limestone. Taking into account the zone of influence and hydrogeological aspects, a deep borehole up to 100 meters below existing ground level was performed under the tower. In advance, it was assumed that CPT would not be able to penetrate sufficiently deep to be directly used for the pile design. In this respect, the decision was made to perform MPTs at depths assumed not reachable by the CPT. All MPTs were performed in the marls. The penetration resistance parameters measured by CPTs covered approximately two thirds of the vertical pile profile. However, the CPT results were considered equally important in terms of site characterization and unit shaft friction evaluation. The scope and type of major in situ tests performed at plot 12 and plot 19 are shown in Figure 2. At plot 12, three CPT tests and one SDMT test were performed. At plot 19, fifteen CPT, eight MPT, and four BD tests were performed. Twenty-two boreholes were drilled, and a significant number of samples were taken to the laboratory for testing. It should be emphasized that only a few samples were retrieved from the ground using the appropriate samplers and drilling tools to achieve quality class 1 according to Eurocode 7 [13]. Those samples were considered to have sufficient quality and were subjected to determination of strength and deformation properties in the laboratory. A good reference to sample quality determination through a change in void ratio can be found in [14]. Borehole logs gave precious insight into the visual determination of geological boundaries and ground model determination.

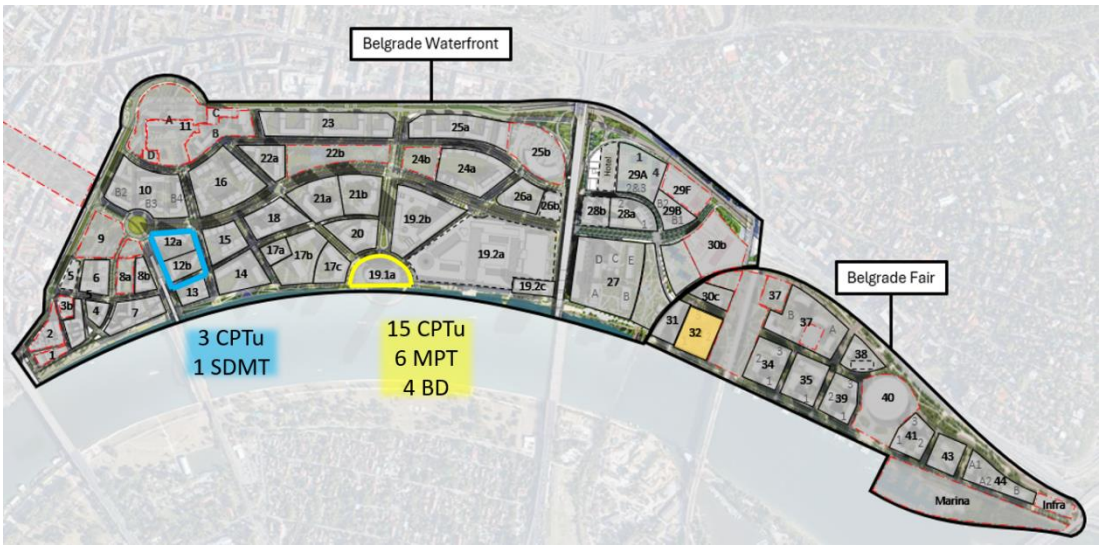

Figure 2. BW masterplan [15].

3.1. The site geology

The BW site is known for its turbulent geological history that produced a complex stress state in sediments in the zone of influence with respect to ongoing construction activities. The zone of influence at the location of the Belgrade Tower is governed by geological conditions, and it is estimated to be approximately 55–60 m below the existing terrain elevation. The general ground model is given in Figure 3 along with pile top and pile bottom elevations for the Belgrade Tower. Previous research related to the BW site can be found in [16–18]. Even if they are similar in terms of lithology, ground models for plot 19 and plot 12 were studied separately due to varying layer thickness.

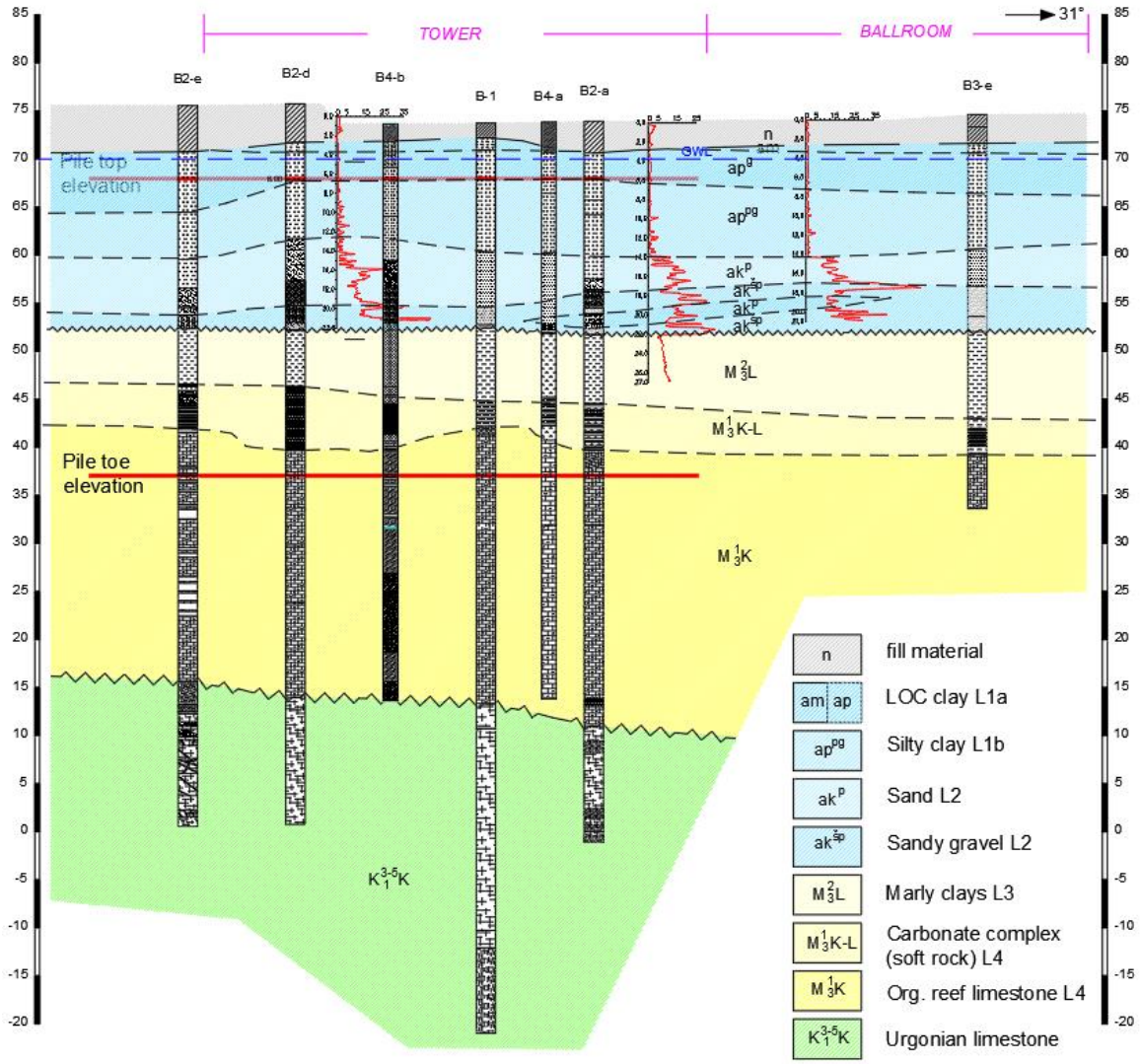

Figure 3. General ground model at the BW site.

The Plot 12 ground model is less favorable in the thickness of soft layers since it is closer to the confluence with the Danube River for approximately 600 meters compared to Plot 19.

The ground model below Belgrade Tower (Plot 19) consists of four major soil-rock layers. The surface layer is composed of fill material that is highly heterogeneous with respect to all geotechnical

parameters. The thickness of the fill material varies across the site, reaching up to 8 meters. Even during the high water season, fill material is mostly above the underground water level. The subsurface layer consists of stillwater/floodplain facies represented by silty to sandy clay (L1). The thickness of this layer is, on average, 8 to 12 meters. Below floodplain sediments, riverbed facies, 7 meters thick, composed of sand and gravel (L2), are found underlain by heavily overconsolidated marls (L3). The thickness of layer 3 is approximately 12 meters. At 30 meters depth, reef organogenic limestone (L4) is encountered. Deep boreholes end in Urgonian limestone, which lies below the reef limestone to significant depths. Urgonian limestone is out of the zone of influence and will not be evaluated further throughout this paper. It should be emphasized that at some locations, fill material had to be removed to perform penetration tests, mainly due to the anchoring capabilities of penetrometers used at the site.

At plot 12, the ground model consists of 6 m of soft, organic clayey fill underlaid by stillwater/floodplain facies, which can be divided into two distinct sub-layers: The top sub-layer of LOC soft clay (L1a), 6 meters thick, and the bottom layer composed of very soft silty clay interbedded with fine sand (L1b), 7 meters thick. Underneath floodplain facies, riverbed sediments (L2), 2 meters thick and composed of sand and gravel, are underlain by 6 meters of thick overconsolidated Miocene marly clay and marl (L3). A non-penetrable soft rock layer (L4) is formed as a sequence of interchanging sandstone, marl, claystone, and limestone layers, and it is found at a depth of 27 meters. At the time of field investigations, the water level was 6 meters below the ground surface.

Soil profiles with index properties and SPT-N blow counts for plot 12 are shown in Figure 4. Water content in the silty clay layer (from 12 to 19 meters) is slightly superior to the liquid limit, which is a typical behavior of sensitive clay, and it can be attributed to its aggregated structure [19,20].

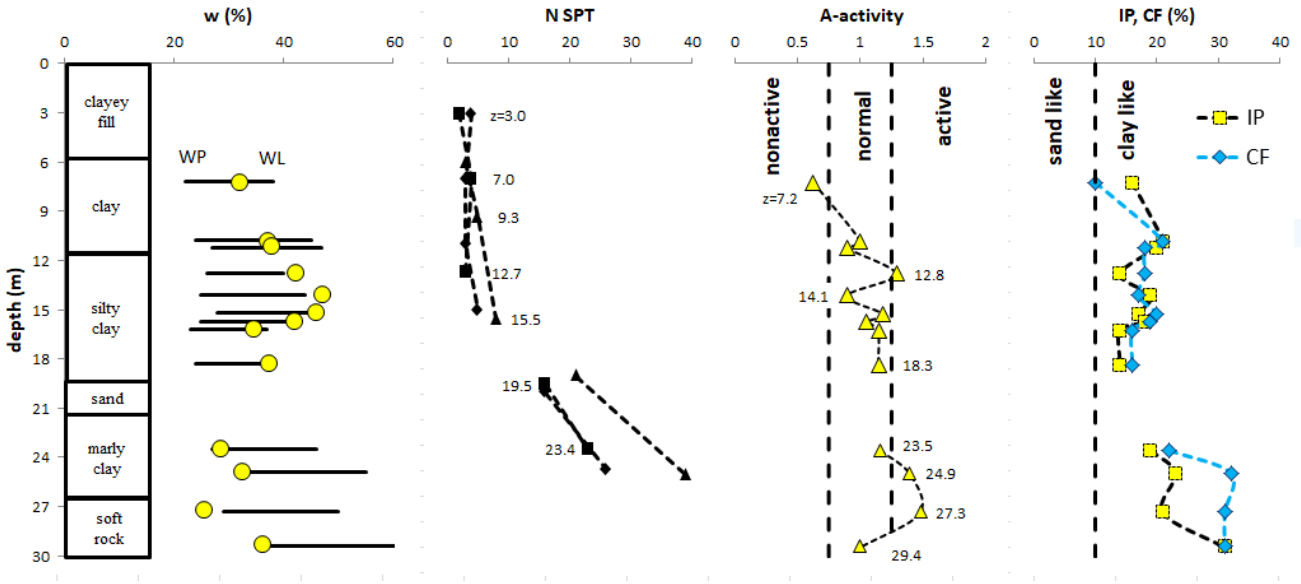

Figure 4. Ground model at plot 12.

The sensitivity of clay estimated from CPT-based correlations [21] is on average 4–5, but it can be as high as 8 at some depths. In marly clays and marls, water content is close to the plastic limit, which is a typical feature of heavily overconsolidated clay. According to Skempton's 1953 activity

chart [22], younger clays encountered at the BW site are classified as normal, while older, Miocene clays have higher activity.

4. Materials and methods

Our purpose of this paper is to intercompare semi-empirical and theoretical correlations that are used to derive soil parameters from CPT, SDMT, and MPT tests. The material used can be divided into four groups: The first group consists of young, lightly overconsolidated clay (LOC) of stillwater and floodplain facies (L1a and L1b). The second group consists of coarse-grained, normally consolidated, riverbed sediments (L2). These two groups are formed during the Holocene. The third group consists of heavily overconsolidated marls (L3) formed during the Late Miocene in a sublittoral depositional environment. The major physical characteristics of the three soil groups are listed in Table 1.

Table 1. Range of physical properties of soil units across the site.

Unit	Clay (%)	Silt (%)	Sand (%)	γ_n (kN/m^3)	d_{60} (mm)	w_l (%)	w_p (%)	w (%)
L1a	8–28	60–84	3–12	19.3	–	31–49	22–28	25–40
L1b	8–33	47–83	3–42	18.9	–	36–63	19–31	26–46
L2	2–6	6–18	60–88	–	0.35–0.46	–	–	19–23
L3	9–42	52–84	3–14	18.7	–	45–68	21–43	19–42

Note: γ_n: bulk unit weight; d_{60}: effective grain size diameter; w_l: liquid limit; w_p: plastic limit; w: natural water content

The data in Table 1 indicate that the L1a layer is more variable in terms of particle size distribution compared to L1b. Relatively high variability of index parameters can be attributed to soil inherent variability.

The fourth group is rock material formed from marly-carbonate soft rock and organogenic reef limestone (L4). Characteristics of this group will be discussed in terms of the BD static load test.

Three methods are used to obtain soil parameters, where two of the methods are based on direct push-in technology: CPT and SDMT, while a third method utilizes the results of pre-bored MPT performed in a previously prepared borehole. The fourth method is a BD static load test on a fully instrumented pile. All methods show insight into soil and rock behavior and the possibility to evaluate engineering properties of natural sediments. Tests are performed using the standardized procedure described by European and American standards. The test standards that were followed were [23] for CPT, [24] for MPT, [25] for DMT, [26] for downhole seismic testing (SDMT), and the BD load test was performed in general compliance with [27].

The major semi-empirical and theoretical correlations used in this study to interpret soil parameters are summarized in Table 2. The applicability of these correlations is discussed further, considering major factors that influence soil behavior during penetration of cone- or plate-shaped tips into the ground.

Table 2. Correlations used to derive soil parameters.

Method	Correlation	Eq. no.	Reference
CPT	$I_c = [(3.47 - \log\ Q_t)^2 + (logF_r + 1.22)^2]^{0.5}$	1	[28]
CPT	$OCR = k \cdot Q_{tn}$	2	[29]
	$k = \left[\frac{Q_{tn}^{0.2}}{0.25 \cdot (10.5 + 7 \cdot log(F_r))}\right]^{1.25}$	3	
	$OCR = \frac{0.33 \cdot (q_t - \sigma_{v0})^m}{\sigma'_v}$	4	[30]
	$m = 0.85\ to\ 1$		
CPT	$K_0 = (1 - sin\varphi') \cdot OCR^{sin\varphi'}$	5	[31]
	$M = \alpha \cdot (q_t - \sigma_{v0})$	6	[29,32]
	$\alpha = 5$ for CPT		
CPT	$I_G = {G_0}/{q_n}$	7	[26,33]
	$q_n = (q_n - \sigma_{v0})$	8	
	$K_G^* = (G_0/q_n)(Q_{tn})^{0.75}$	9	
CPT	$I_R = exp\left(\frac{2.93 \cdot B_q}{1 - B_q}\right)$	10	[34]
DMT	$I_D = (p_1 - p_0)/(p_0 - u_0)$	11	[35]
	$K_D = (p_0 - u_0)/\sigma'_v$	12	
	$E_D = 34.7 \cdot I_D \cdot K_D \cdot \sigma'_v$	13	
DMT	$s_u = 0.22\sigma'_{v0}(0.5K_D)^{1.25}$	14	
DMT	$OCR = (0.5K_D)^{1.56}$	15	
DMT	$K_0 = (K_D/1.5)^{0.47} - 0.6$	16	
DMT	$M = E_D R_M$	17	
	$R_M = f(I_D, K_D)$	18	
MPT	$\tau = dp/d[ln(\Delta V/V)]$	19	[36,37]
	$\gamma \approx 2\varepsilon_c = 2[(1 - \Delta V/V)^{-0.5} - 1]$	20	

Note: Normalized CPT parameters are defined as follows: $Q_t = (q_t - \sigma_{v0})/\sigma'_{v0}$, $F_r = \left[\left(f_s/(q_t - \sigma_{v0})\right)\right] \cdot 100\%$, $B_q = (u_2 - u_0)/(q_t - \sigma_{v0})$, $Q_{tn} = \left[\frac{q_t - \sigma_{v0}}{p_a}\right]\left[\frac{p_a}{\sigma'_{v0}}\right]^n$ and $U_2 = (u_2 - u_0)/\sigma'_{v0}$

5. Test results and comparison

Besides soil type and state, major factors that influence penetration resistance are the rate of penetration, microstructure (bonding and cementation), and shape or geometry of the probe. The influence of probe geometry on penetration resistance parameters has been studied numerically and experimentally [38–42]. [43] and [44] show that the blunter tips push soil down as they penetrate like a rigid punch, indicating that q_c is largely a result of normal stresses acting on the probe tip. In contrast, the sharper tips push the soil radially away from the tip like an advancing wedge, with tip resistance

originating mostly from frictional resistances at the soil-tip interface. The latter corresponds more to the shape of the dilatometer, indicating large differences in the stress-strain field around cone- and blade-shaped probes. In contrast to V_s or G_0 measurements, CPT and DMT parameter evaluation is based on the disturbed soil state. This so-called disturbance effect imposes additional uncertainty in the derivation of engineering properties from penetration tests. In recent years, a combination of small (V_s and G_0) and large strain parameters (q_t, M and K_D from DMT) have been used for better understanding and characterization of sediments.

5.1. Partial consolidation effects

The rate of penetration is linked to the consolidation or flow characteristics of the soil [39,45,46]. Generally, it is accepted that a standard penetration rate of 2 cm/s and standard cone geometry cause undrained penetration in clay and drained penetration in free-draining soils (sands). Most of the correlations used to interpret soil parameters from penetration tests are derived for fully drained or fully undrained penetration conditions for the standard penetration rate [29]. For varying penetration rates [46], it was found that the ratio of drained to undrained cone resistance can be as high as 17 for the sand-kaolin mixture. In this study, penetrations are performed using a standard cone (10 cm²) or blade and standard penetration rate; thus, drainage conditions around the probe during penetration are governed solely by the coefficient of consolidation of a soil. In that respect, it should be mentioned that penetration in L1a is undrained. Moreover, L1b is interbedded, and drainage characteristics are very complex, and for some depths can be partially drained, as shown later. In L2, penetration is drained, while in marls (L3), penetration is considered undrained due to its low permeability.

There are several recommendations in terms of test procedure if partial drainage influences the interpretation of penetration tests, such as those recommended in [47–50], which recommend performing a short A-dissipation test at several depths during DMT sounding so the development of pore pressures around the membrane can be followed in time. If an A reading changes during the time needed to perform the standard DMT test (e.g., 30 seconds for A and B), then the B reading, which follows A, is not an adequate match for A. This would influence all parameters derived from the difference of the two readings, B-A, and in some cases, the A reading is influenced by pore pressure dissipation by an unknown amount. Based on the method recommended by [50], [18] showed that when the standard DMT interpretation procedure is used to derive soil parameters, undrained shear strength (s_u) is more influenced by partial drainage than constrained modulus (M). This can be attributed to the fact that s_u is derived solely from corrected A readings (p_0) compared to M, which is derived from p_0 and p_1 readings. This highlights the importance of understanding partial drainage influence on soil parameters derived from either CPT or DMT tests.

In Figure 5, the profile of DMT pressures (p_0, p_1, and p_2) is shown along with three short A-dissipation tests performed at different elevations. It can be observed that for the test at 18.4 meters, A decays much faster compared to the other two tests, indicating a faster dissipation of pore pressures around the membrane. In these situations, to reduce uncertainty in the derivation of soil parameters from standard DMT correlations, correction of measured DMT field data can be made according to the procedure described in [50].

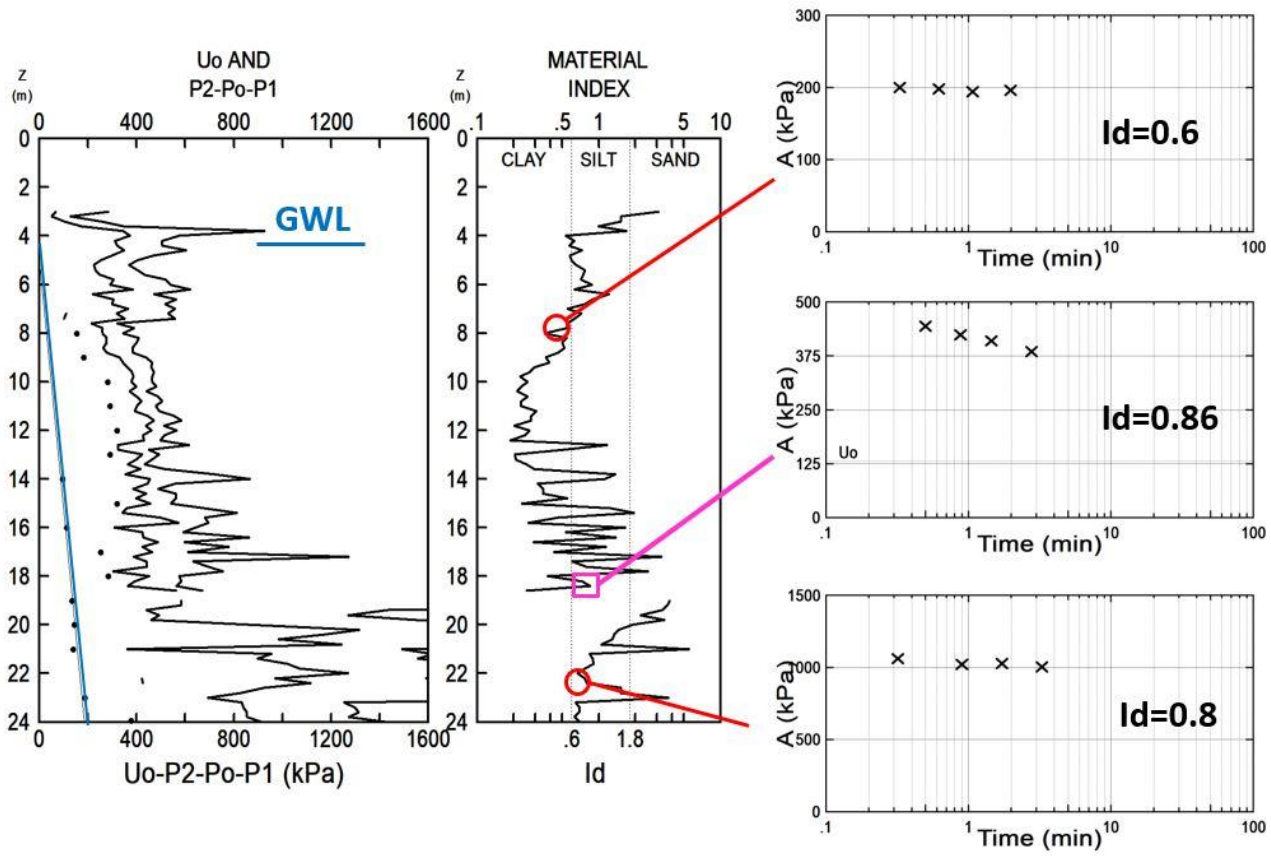

Figure 5. Corrected pressures and a short A-dissipation test at three levels.

5.2. Detection of microstructures

All soils can be considered to have a microstructure that is more or less pronounced depending on the depositional and post-depositional processes that a particular soil has undergone during its geological life. Microstructure is used as a term to describe soils that have unusual characteristics compared to ideal soil, which have little or no microstructure. There are several approaches, utilizing in situ tests, that can be used to determine the presence of microstructure in a soil. [51] showed that results from CPT in soils with significant microstructure can be described differently by soil behavior type-normalized (SBTn) Q_{tn}–F_r and Q_{tn}–U_2 charts. If seismic CPT is used for testing, then an additional method, based on a small strain rigidity index (I_G) (Eq. 9), can be used to discern soils with and without a microstructure. Using geological evidence and knowledge of the geological history of a specific geotechnical unit, along with laboratory tests, it was demonstrated by [52,53] that microstructure can be identified by comparing the measured and estimated Vs profiles.

Estimation of V_s profiles can be done utilizing some of the commonly accepted correlations for CPT and DMT tests (e.g., [28,54,55]). Most correlations for the interpretation of in situ tests are evaluated for young, normally consolidated soils. Shear wave velocity is more sensitive to ageing and cementation compared to large strains induced by a penetrating cone or blade since shear waves produce small strains in a soil. Results obtained for paired CPTu and SDMT on plot 12 are shown in Figure 6 concerning four SBT type charts that can be used to identify soil with a significant

microstructure. Two of those charts (Figure 6a and 6b) utilize normalized CPT parameters Q_{tn}–F_r and Q_{tn}–U_2, while charts in Figures 6c and 6d are based on Q_{tn}-G_0/q_n and I_D-K_D. Both charts, in Figures 6c and 6d, use V_s or G_0 to detect microstructure. In Figure 6e, a comparison of measured SDMT-V_s and estimated CPT-V_s profiles is shown. Shear wave velocity is estimated using correlation from [28].

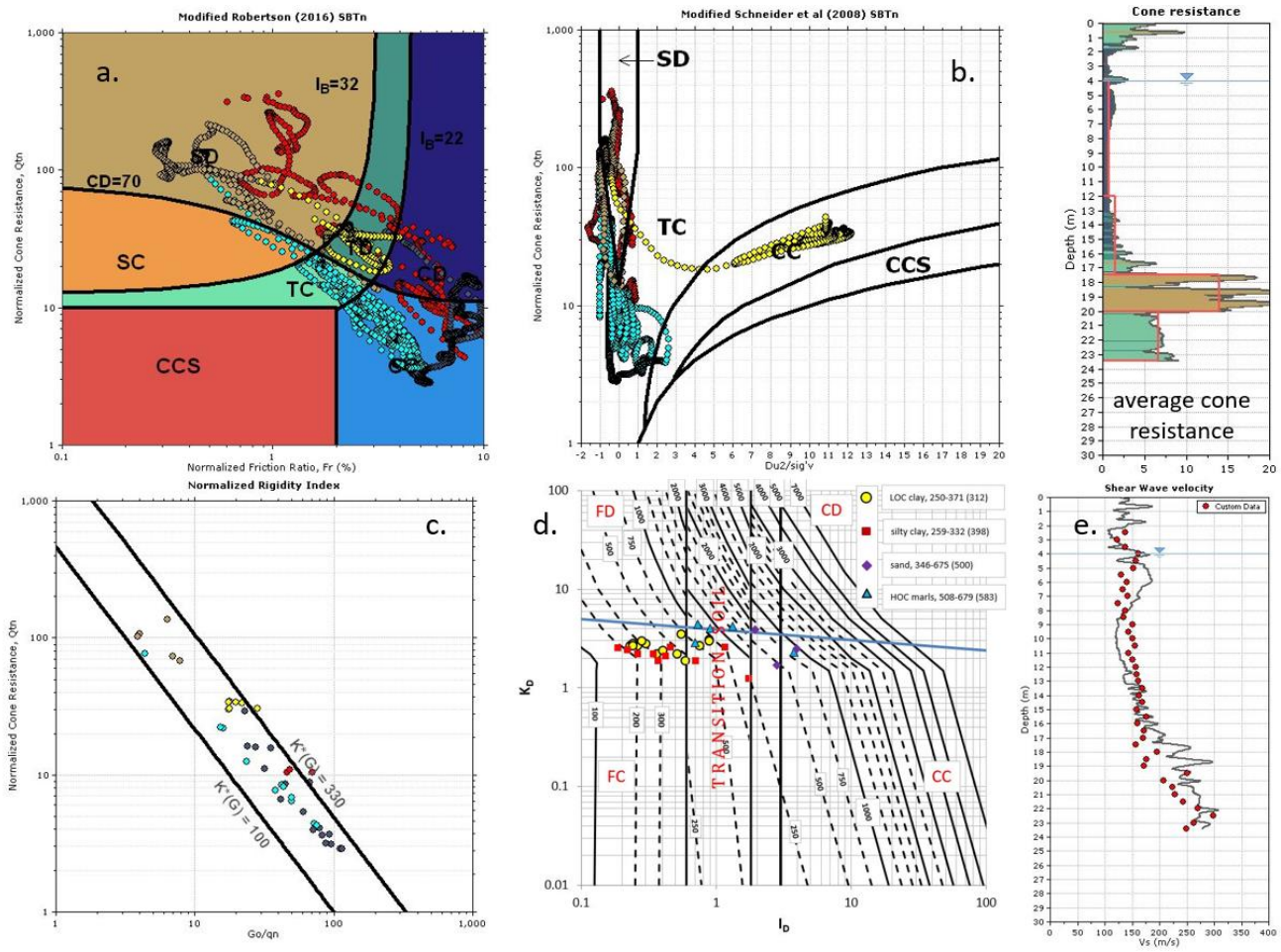

Figure 6. Microstructure SBTn charts from CPTu and SDMT test results with test results from plot 12 (point colors for a to c: Red-fill; dark blue-L1a; light blue-L1b; brown-L2; and yellow-L3), Du2/sig'v=U_2 (Table 2).

Important points to consider with respect to Figure 6 are discussed next. Penetration pore pressure, measured at u_2 position, reach their maximum value of 2.35 MPa when the cone penetrates HOC marls. This maximum value represents the upper bound of the measuring range of the cone used. Similar results have been reported by [56] for Miocene lacustrine clay of the same origin but at different locations. For this particular clay at plot 12, the u_2/u_0 ratio is larger than 13. Pore pressure parameter B_q is on average 0.35, while U_D = 0.26-0.3 in marl (excluding sandy interbeds). By comparing the Q_{tn}–F_r and Q_{tn}–U_2 graphs (Figure 6a and 6b), it can be seen that points representing results in marl (yellow dots) plot in the TD and CC zones, respectively. According to [51], if data is plotted in the region represented by $Q_{tn} > 20$ combined with high positive U_2 values ($U_2 > 4$), the soils likely have significant microstructure (i.e., structured soils) and are contractive at large shear strains. For marls at plot 12,

$Q_{tn} > 20$ and $U_2 > 6$, indicating a soil with microstructure. Microstructure in marls is a consequence of carbonate cementation developed at the contact of clay aggregates and silt grains. According to the values of Q_{tn} and U_2 for other soil layers at plot 12, the microstructure is less pronounced. Figure 6c indicates that in Pannonian marls, $K_G^* = 320$ and is higher compared to Holocene-age sediments, where $K_G^* = 230$. According to [51], higher values correspond to older sediments. Figure 6d represents the microstructure SBT graph used when SDMT results are available. This graph is suggested by [57], and it was further developed by [52] and [58]. The graph is divided into four zones: FC-fine-grained contractive, CC-coarse-grained contractive, FD-fine-grained dilative, and FC-fine-grained contractive, describing soil behavior depending on the two DMT intermediate parameters I_D and K_D. The transitional zone is delineated by a material index I_D between 0.6 and 1.8, indicating soil that exhibits partial drainage during testing. However, care is advised if partial consolidation is assessed only from I_D. This is supported by the results shown in Figure 6, where a significant difference in decay of A for $I_D = 0.8$ and $I_D = 0.86$ can be observed. Results for the marl plot in the transitional zone close to the blue line represent the boundary between dilative and contractive soils. Similar results are obtained from CPT (Figure 6a), where data for marl plots close to the CD = 70 boundary show slightly more dilative behavior. Comparing Figures 6a and 6d, a similar description among other geotechnical units can be seen in terms of behavior at large shear strains (e.g., dilative-contractive), confirming that both tests, CPT and DMT, describe soil in a consistent manner.

In Figure 6d, black lines represent the estimated G_0/σ_v' ratio. According to [52], if the measured and estimated G_0/σ_v' ratio differs considerably, it indicates significant microstructure in a soil. The range of measured (and average) G_0/σ_v' ratios for each soil layer are shown on the key in Figure 6d. It can be observed that the greatest difference is for marls, which is consistent with the V_s profile shown in Figure 6c and 6e.

CPT results for plot 19 are shown in Figure 7 on Q_{tn}–F_r and Q–U_2 charts only since SDMT was not performed, and there are no seismic measurements. Unlike the modified Schneider's chart shown in Figure 6b, Figure 7 uses the original Schneider's soil classification chart. At plot 19, two CPT penetrated the marls. On the Q_{tn}–F_r chart, points plot on a sand-like dilative region, while from the Q–U_2 chart, marl is classified as a clay having large pore pressures developed during penetration. Higher values of $Q_{tn} > 30$ and $U_2 > 13$ are measured at plot 19 compared to plot 12, indicating a more pronounced microstructure. Compared to plot 12, at plot 19, a larger B_q (=0.5) is measured in marls since a cone of a different manufacturer was used. Even so, the upper bound of the pore pressure measuring range (=4.7 MPa) is reached at some depths.

Application of correlations used to interpret soil parameters from CPT and DMT will be examined further throughout the manuscript by taking into consideration the presence of a microstructure in a soil and partial drainage effects.

5.3. CPTu vs SDMT comparison

5.3.1. Stress history

Initially, all sedimentary soils are normally consolidated. However, as a result of its exposure to a variety of physical and other processes over many thousands to millions of years, tmost become

overconsolidated. Various mechanisms induce preconsolidation in the soil, including overburden erosion, ageing, rise in underground water level, glaciation, freeze-thaw cycles, repeated wetting-drying, desiccation, earthquake loading, cementation, and other factors [59]. In this respect, the first step toward understanding soil behavior would be a quantification of the yield stress profile of the material and the stress history. Fundamental stress history parameters that influence soil behavior regarding strength and stiffness are yield stress ratio (YSR = σ_y'/σ_v') or overconsolidation ratio (OCR) and lateral stress index at rest (K_0).

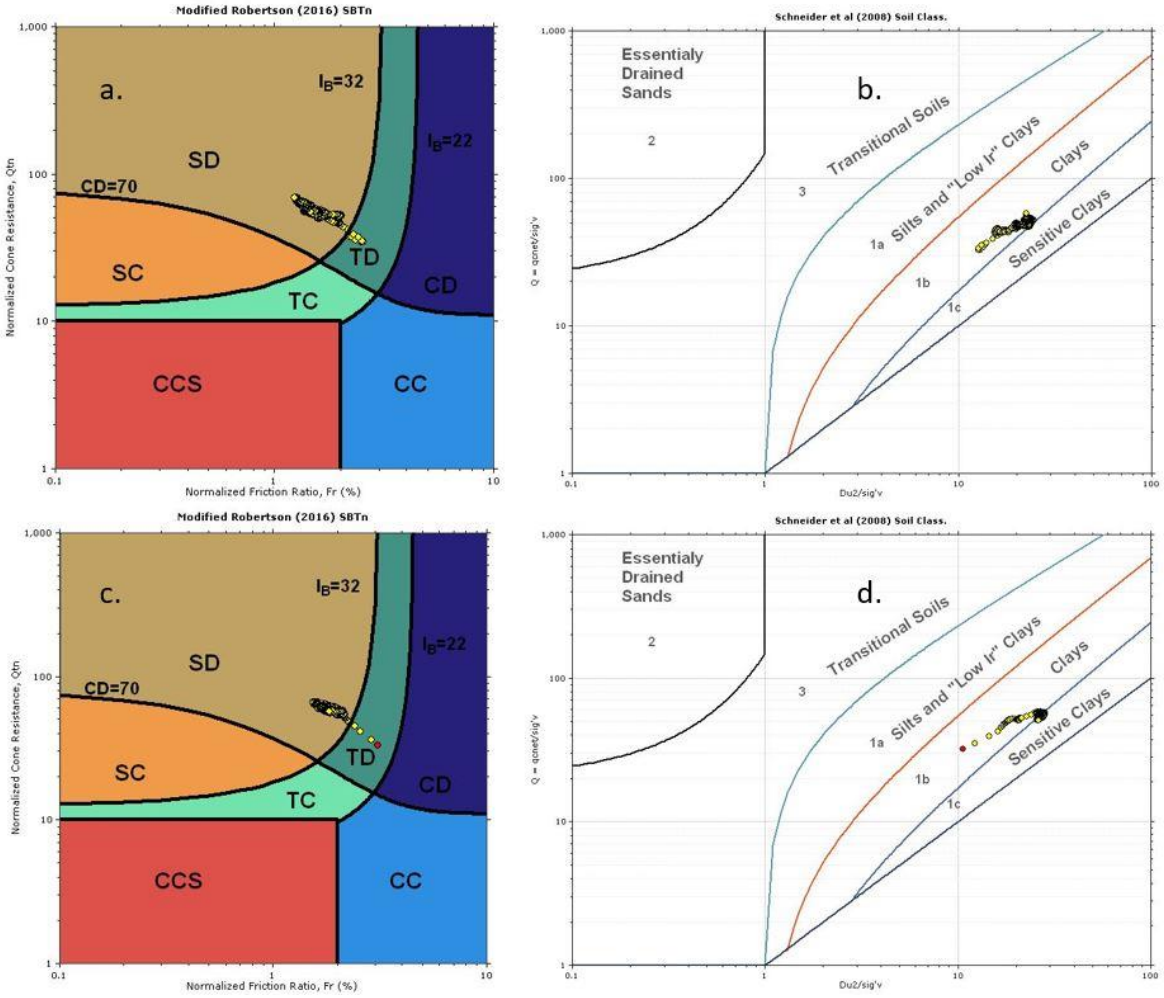

Figure 7. Results in marls from plot 12 obtained by two CPTs presented at the modified SBTn chart [51] and Schneider's soil classification chart [60].

The reference test for determining the YSR is the oedometer test, where K_0 stress conditions prevail. Several methods can be used to determine the yield stress for soil samples from an oedometer, among which the graphical Casagrande method is the most common. In our study, the Casagrande method was used.

Construction activities and geological evidence indicate that (L1a) have apparent preconsolidation caused by two major factors: (1) The underground water level is raised for two meters after construction of HPS Đerdap, and (2) the weight of fill material produces a constant load over

time, which causes consolidation and creep of clay below the fill. Additional load causes ageing of initially young, normally consolidated clay deposits at the site. Instead of using the term OCR, the term yield stress ratio (YSR) is employed since apparent preconsolidation for LOC clays is a consequence of the combined factors mentioned previously. A YSR vs depth profile determined from odometer testing is shown in Figure 8a for plot 12.

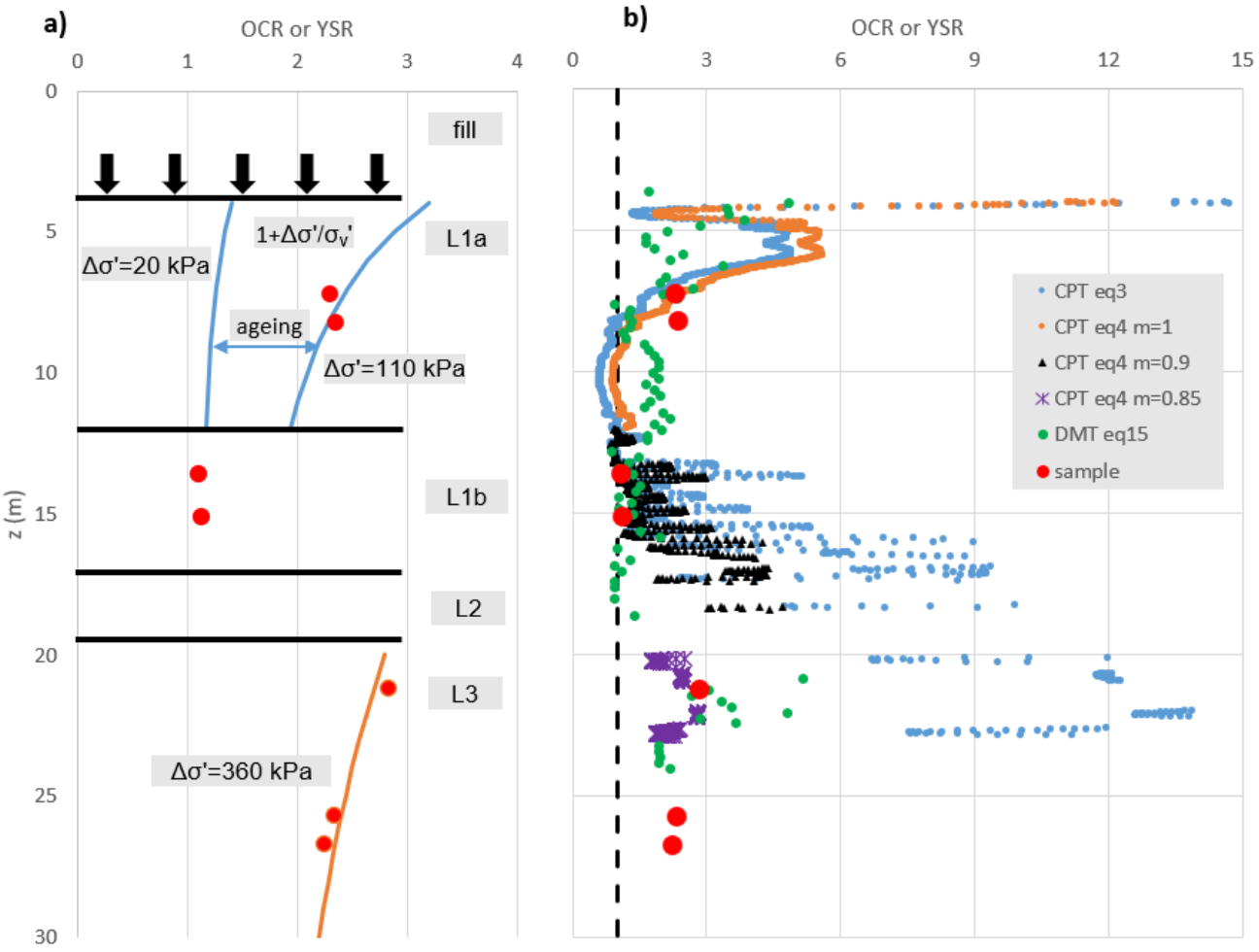

Figure 8. YSR profile at plot 12 determined by: a) Odometer test, and b) CPT-SDMT correlations (Eq. 2, Eq. 3, Eq. 4, and Eq. 15).

Seven odometers, with sufficiently large stress levels after preconsolidation stress, were used to determine YSR. Figure 8 shows YSR determined from soil samples as points, while continuous lines represent its distribution derived from the indicated stress difference ($\Delta\sigma$). Strictly speaking, the formula shown in Figure 8a should be used only when a deposit is mechanically, one-dimensionally unloaded. The YSR profile derived from $\Delta\sigma$ = 20 kPa approximately corresponds to an increase in water level at the site. If this was the only mechanism producing preconsolidation, YSR would slowly decrease with depth to unity in an L1b. However, a larger stress difference ($\Delta\sigma$ = 110 kPa) better fits experimental data. This indicates that other mechanisms are involved in producing larger yield stress in an L1a. As mentioned, it is assumed that ageing is a major cause. A significantly larger stress

difference should be used to fit experimental data for L3. At the BW site, marls are moderately to heavily overconsolidated, and this is a general feature of a Belgrade marl. Several authors provide evidence of the thickness of overburden that was eroded due to vertical tectonic movements that took place during the late Miocene, exposing marls to atmospheric influences. The thickness may vary from 50 m to 250 m in the Belgrade area [61]. In addition to preconsolidation that increases pseudo-elastic range, marls are soils with significant microstructure that originates from carbonate cementation, having 10% to 60% carbonate content in this case. Carbonate content is known to increase the stiffness and strength of a soil [62,63]. In this respect, marls have apparent preconsolidation that comes from the combined influence of mechanical erosion and cementation. Exact quantification of the individual influences that these two factors have on preconsolidation is difficult. This is important in terms of the interpretation of in situ tests.

In addition to laboratory tests, YSR is evaluated from CPT and DMT correlations shown in Table 2. Two CPT methods are used. The first method uses a variable k factor defined by equation 3 [29], while the second is based on a constant k = 0.33 with a variable m factor [30]. [30] showed that the m factor depends on the soil type. For young, uncemented soils, m can be evaluated from the material index (I_c), while for other soils (e.g., with microstructure), this procedure is less reliable, and it should be based on direct comparison with laboratory test results. YSR from DMT is evaluated using equation 15 [64].

From Figure 8b, it can be seen that the DMT standard interpretation procedure closely predicts YSR. Equation 3 underpredicts YSR in L1a and significantly overpredicts YSR in L1b and L3. Equation 4 closely predicts YSR using different m factors for different layers, as indicated in the figure.

5.3.2. Soil type

At plot 12, a pair of CPT-SDMT is performed at a distance of 1.5 meters. A comparison of soil behavior type indices (I_C-I_D) derived from two tests is shown in Figure 9a, along with soil descriptions from adjacent boreholes, natural water content and plasticity limits. SBT zones (2 to 7) from [65] are indicated on the I_C graph. Comparison of I_C and I_D vs depth graphs indicates an overall good match of soil type delineated from CPT and SDMT, following a similar trend with depth. Silty clay layer (L1a) is interbedded with silty sand, with increasing sand fraction vs depth and gradual transition to the sand layer below. This behavior is confirmed from the borehole log and is correctly indicated by both indices. However, there is some discrepancy in soil type evaluation at depths of 17 to 19 meters, which can be attributed to spatial soil variability.

5.3.3. Modulus prediction from penetration tests

The flat dilatometer test (DMT) has often been shown to provide excellent estimates of settlement using predicted values of 1-D constrained modulus [58,66]. Parallel CPT-DMT soundings enable us to graph parameter α vs depth using constrained modulus (M) derived from DMT correlations employing equations 17 and 18 from Table 2.

The vertical profile of α, defined as a ratio of constrained modulus and net cone resistance, is shown in Figure 9b. Approximate average values of α are marked for each layer as a vertical line on the graph. It is observed that α depends on OCR. For LOC clay up to 12 meters depth, α is on average

10, while in NC silty clay layers, α reduces to an average value of 5. The latter value agrees with recommendations proposed by [32] as an average value for "well-behaved" soil. Low α is noticed for depths ranging from 17 to 19 meters, which can be attributed to local variations in soil type, as mentioned before. Derivation of α in the sand layer is disputable due to its relatively small thickness. The first meter of marl is very stiff and coarser compared to the lower part, with K_D ranging from 4 to 6. On average for this upper part, α = 13, while deeper parts have a more common value of 5. When assessing parameter α, it is advised not to compare the results at a single point at some depth but to inspect profiles of M and (q_t-σ_v) vs depth due to soil variability and different measurement intervals of the two tests. Figure 9c compares the constrained modulus obtained from odometer tests with interpreted modulus from CPT (Eq. [6]) and SDMT (Eq. [17] and Eq. [18]). It is observed that, for a practical application, there is a good fit between the reference laboratory and estimated data from penetration tests. The modulus presented in Figure 9c corresponds to in situ vertical effective stress σ_{v0}' at the test depth.

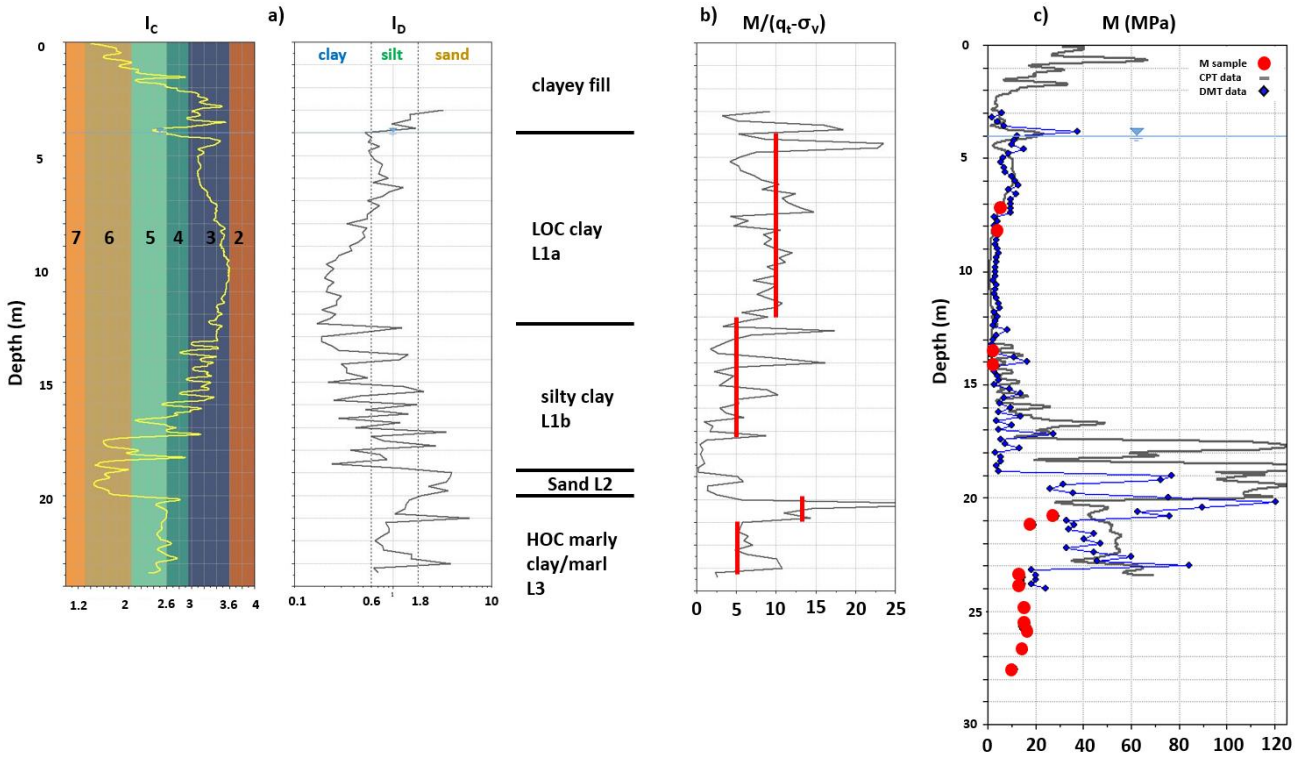

Figure 9. Test comparison: a) Soil type estimated from CPT and DMT (numbers on I_C graph indicate SBT zones), b) α profile (Eq. [6]), and c) modulus comparison.

5.4. Interpretation of the MPT

MPT is a stress-controlled device used to carry out in situ tests of soils for strength and stiffness parameters. The probe used is a G-type probe that expands the membrane radially in a vertical borehole, deforming soil up to 40% cavity strain (ε_c). In ideal conditions where borehole radius is the same as a pressuremeter radius, this cavity strain is sufficient to reach the Menard limit pressure (p_{lM}) or the pressure where the size of the pocket doubles. The p_{lm} should not be confused with the theoretical limit

pressure (p_l) reached at $\Delta V/V = 1$ or where the cavity expands indefinitely. It should be remembered that MPT is installed into a pre-bored pocket where material local to the cavity pocket will be in a different condition from the undisturbed material further away in the soil. Moreover, removal of the boring tool causes reverse plastic failure. However, if the volume of material loaded by the pressuremeter exceeds the volume of disturbed material by a sufficiently large amount, then the measured results reflect undisturbed soil conditions. When interpreting pressuremeter tests, soil is considered either as elastic, perfectly plastic, or elastic strain hardening/softening material since cavity expansion and contraction solutions have been derived for these materials. It is assumed that the soil is fully saturated, and the volume remains constant (undrained test) or that there is no change in pore pressures and the volume of soil changes (drained test). Standard interpretation of pressuremeters involves a small-strain theory, even if some pressuremeters (e.g., Menard type) expand soil up to 40% cavity strain. All mentioned assumptions present practical limitations of the interpretation of pressuremeter tests.

At plot 19, MPTs were performed as a complement to CPT tests since most of the CPTs could not penetrate stiff marls. The layout of field investigations performed at plot 19 is shown in Figure 10.

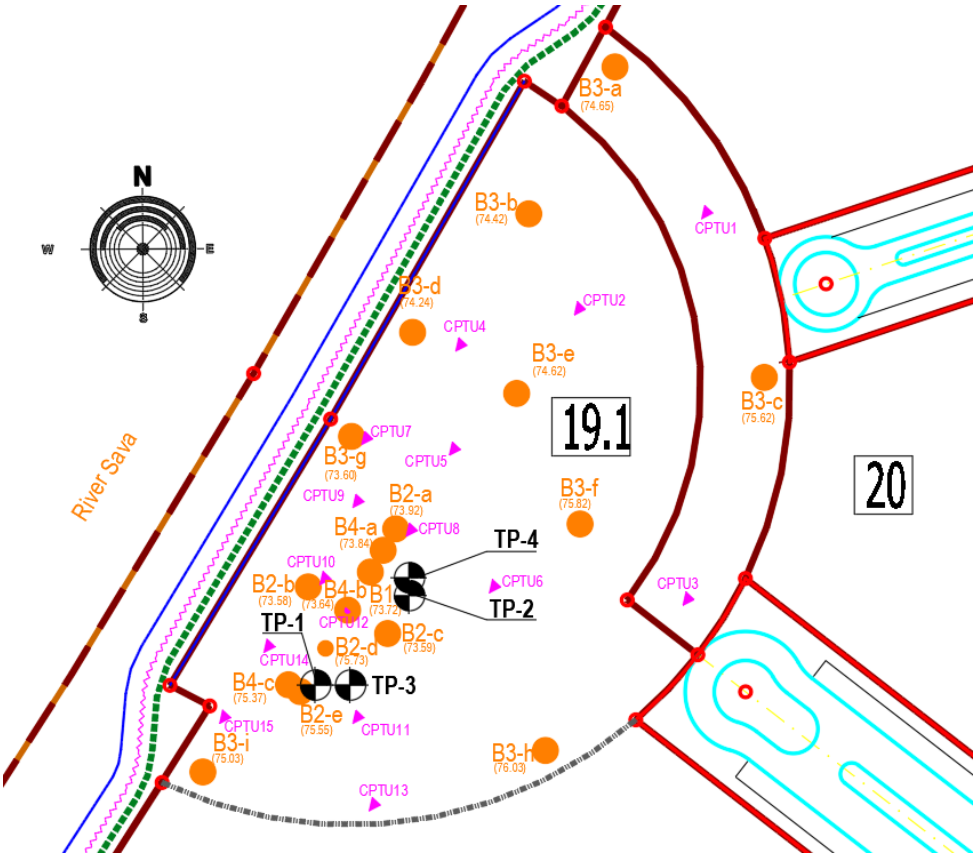

Figure 10. Layout of field investigations for the Belgrade Tower at plot 19.

Two major parameters derived from MPT are p_{lm} and Menard modulus (E_M), used mainly for geotechnical design on an empirical basis. In addition, yield stress (p_f) is an important parameter for the interpretation of the test. It is calculated to check the quality of the test or to estimate p_{lM} when this value

cannot be assessed directly [67]. One of the major challenges when interpreting MPT is the estimation of in situ horizontal stress (σ_h). Several techniques exist that are used to estimate σ_h [68]. Some are developed specifically for pre-bored pressuremeters (e.g., MPT). The method developed by [37] for stiff clays based on peak strength and yield stress is used in the paper. Corrected volume-pressure and creep curve for the MPT performed in a borehole Bh3 at 22.5 m depth are shown in Figure 11a. Figure 11b shows the selection of the pseudo-elastic range of pressure over which E_M is calculated, where parameter m_i is the slope of a linear segment between two adjacent data points [24]. Each of the tests performed at BW is interpreted in a similar and consistent manner following the procedure suggested by [24].

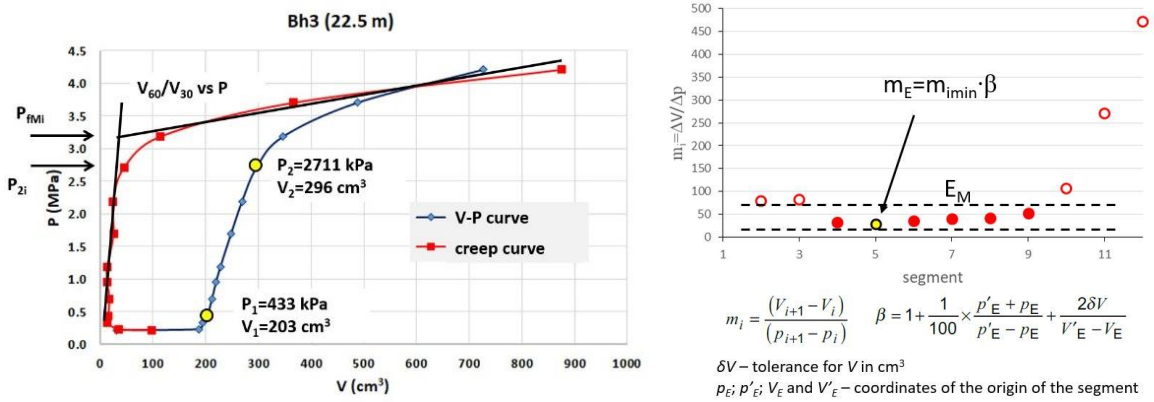

Figure 11. Interpretation of the Menard pressuremeter test: a) Corrected volume-pressure and creep curve, and b) pseudo-elastic range selection for E_m determination.

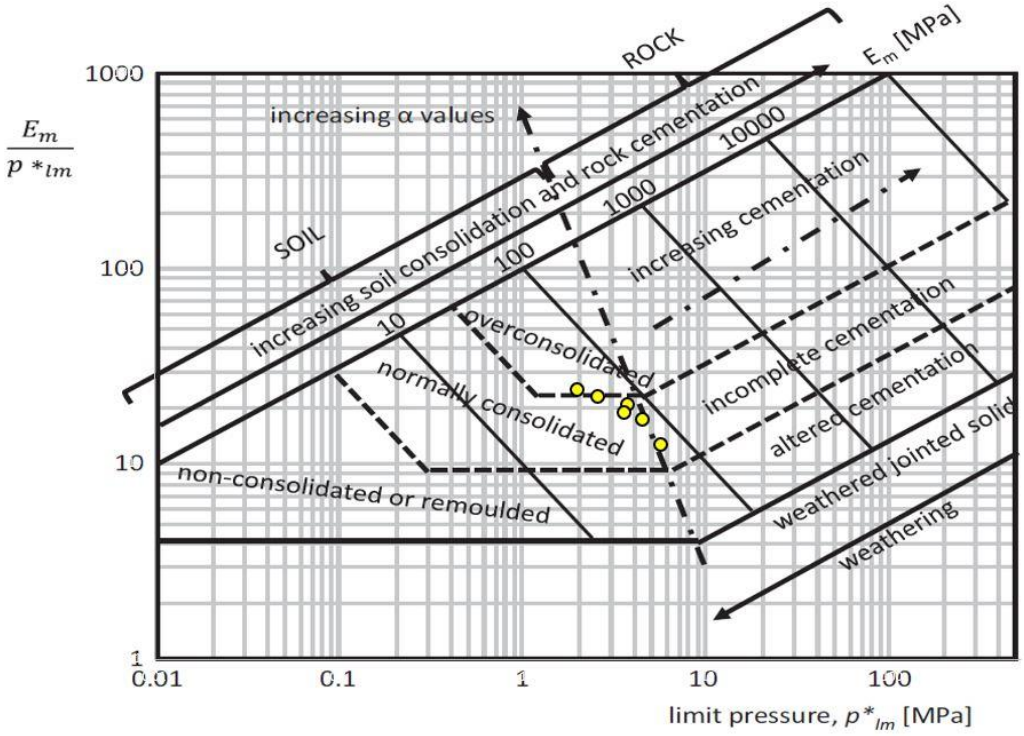

Figure 12. Soil type from MPT according to the pressiorama chart [69].

The soil type determined from MPT is shown in Figure 12. When compared to results obtained from CPT shown in Figure 7, it can be seen that both charts indicate that marl is "transitional material" with characteristics of hard soil-soft rock behavior. The MPT results plot on three different groups of ground on the pressiorama chart close to the soil-rock boundary.

It can be argued that the position of the soil-rock boundary on the pressiorama chart should be slightly modified to fit our data better. The boundary between normally and overconsolidated soil indicated by the normalized parameter E_M/p^*_{lM} should be lower, and it should be approximately at $E_M/p^*_{lM} = 20$. The boundary between soil and rock should be slightly shifted toward the origin. In this way, marls would be classified as cemented material, which is in accordance with CPT results.

Additional interpretation of MPT is performed using the [37] procedure for σ_h estimation. The procedure is applicable to stiff clays with significant linear elastic behavior that show marked yield points. It is based on the premise that the elastic response of the soil should cease when the undrained shear strength in the wall of the cavity is reached. At that moment, the sum of the peak shear strength (s_u) and σ_h are equal to the yield stress (p_y). The method uses iterative graphical procedures to find s_u and σ_h and is sensitive to the choice in reference volume V_0. Results of the application in [37] to the test performed in a borehole Bh3 at 22.5 m (Figure 11) are shown in Figure 13. Four iterations are performed for different initial estimates of σ_h. For example, it can be observed that for the first iteration, the p-ε_c curve is linear well past the pressure p_y. Iteration 2 gives the closest match for an initial assumption made with respect to total horizontal stress (σ_h = 701 kPa). This σ_h would correspond to a value of $K_0 = 2.8$. Interpreted values of K_0 using the [37] procedure range between 2.1 and 3.2. High values of K_0 indicate that marl is heavily overconsolidated at the location of the Tower. Undrained strength interpreted from the maximum slope of the pressuremeter expansion curve is s_u = 1.4 MPa. High peak s_u values could not be confirmed from laboratory tests due to a lack of good-quality samples. Further, more details on shear strength derived from pressuremeter tests will be presented.

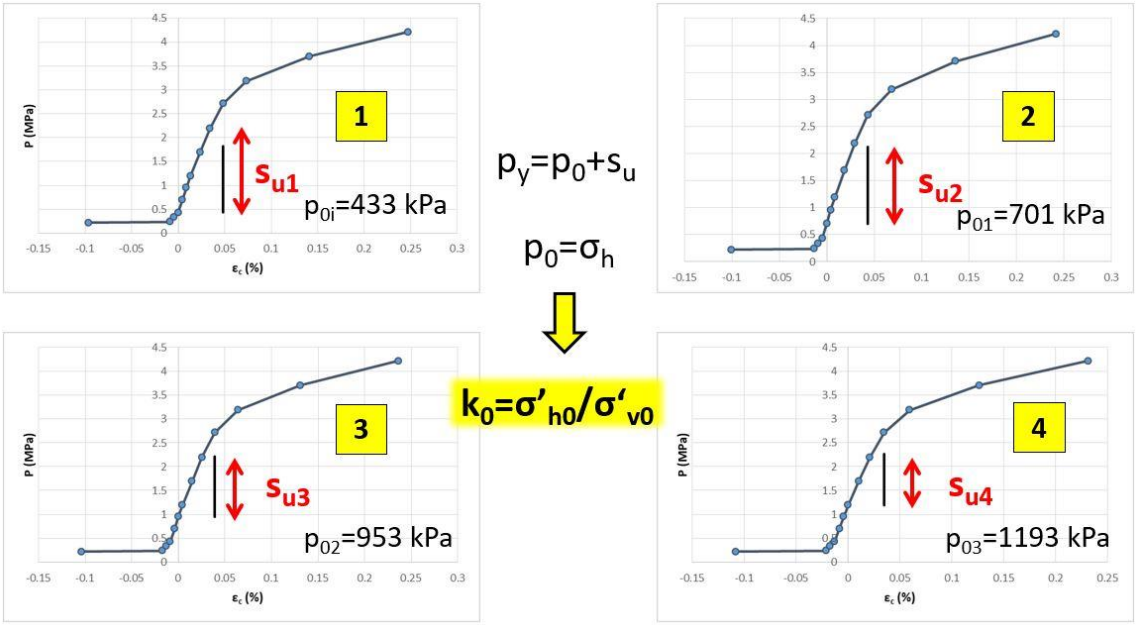

Figure 13. Graphical estimation of σ_h from MPT results using the procedure from [37].

In theory, the precise form of the shear stress-shear strain curve can be deduced from measured pressure-cavity strain [36]. Equations 19 and 20 state that the shear stress (τ) at a particular cavity strain is equal to the current slope of the plot of p-ln(ΔV/V) shown in Figure 14a. The use of equations 19 or 20 requires that curves constructed from experimental data points should be differentiated to find their slopes. For the MPT test, this would be practical only if a mathematical function is used to fit the experimental curve. Then, using the slopes of that smooth function, shear stress could be determined. Since MPT is performed in 8 to 14 increments of pressure, an assumption has to be made with respect to interpolation between two adjacent data points. If secant values are used (the difference between two adjacent measurements), the results shown in Figure 14b are obtained. Figure 14 indicates that marls at BW show typical behavior of stiff clays with peak shear strength significantly higher compared to ultimate or residual strength at very large strains. Only three MPTs are interpreted in terms of shear stress-strain behavior since, for other tests, data are more erratic. As shown in the figure, reference shear strain (γ_{ref}) at peak shear stress is approximately 7%. If the rigidity index (I_R) is considered as a reciprocal of $\gamma_{ref,}$ then I_R = 14 for peak shear stress. In addition to MPT, I_R can be evaluated from CPT using B_q (Eq. 10 in Table 2). For plot 19, B_q = 0.5, which corresponds to I_R = 18 and is similar to the value obtained from MPT, with a tendency of I_R to decrease with increasing OCR/YSR [59]. This finding is in accordance with the heavily overconsolidated nature of the marls at plot 19. Moreover, for low I_R material, shear-induced pore pressures have a greater effect on the measured penetration pore pressures (u_2).

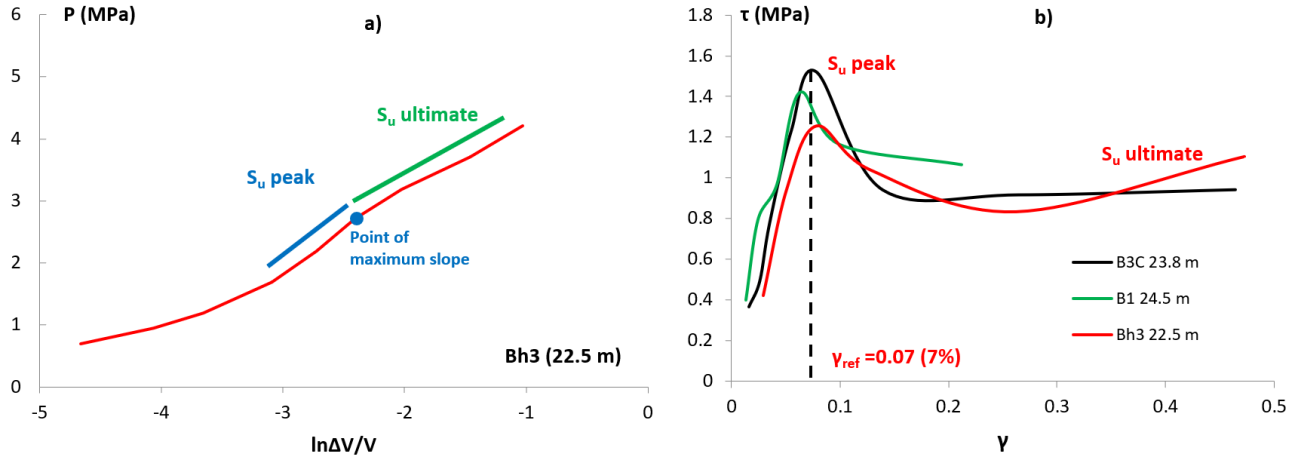

Figure 14. Shear stress-cavity strain curve from slope of pressuremeter expansion.

5.5. Bi-directional static load test

At plot 19, four BD static load tests on fully instrumented piles were performed. The pile test layout is shown in Figure 10. Piles TP-1 and TP-2 were poorly constructed, and evaluation of test data was difficult and inconclusive. Two additional piles, TP-3 and TP-4, were tested to a maximum load of 61.78 MN in 18 equal increments (IL). According to our knowledge, this is the first BD test performed in Serbia and the largest load applied to any pile in the region. More details regarding test results and numerical simulation can be found in [16,17]. In this paper, we focus on shaft distribution in marls and organogenic

reef limestone measured from BD tests. Figure 15 shows load distribution in pile TP-4 as measured by the strain gauges (SG) placed at different elevations along the pile.

Mobilized shaft friction in marls, marly complexes, and reef organogenic limestone is shown in Figure 16. If mobilization of q_s in marls is considered (pile element between SG4 and SG5), it can be seen that q_s linearly increases up to 1.5 mm, which corresponds to 0.12% of the pile diameter (D). Numerous static load tests performed on instrumented piles indicate that full shaft friction is mobilized at a relative pile movement of 1% diameter (0.01·D). In this respect, full q_s is mobilized for pile elements between BD-SG2 and SG2-SG1, as shown in Figure 16. For other parts of the pile, q_s is not fully mobilized. It is significant to note that the limestone shows strain-softening behavior during loading with softened shaft friction corresponding to approximately 60% of the peak load.

Numerical values of unit shaft friction (q_s) mobilized at a maximum movement of the pile element for the last load increment 1L-18 of the first load cycle are shown in Figure 15. These values are used as reference values for further discussion.

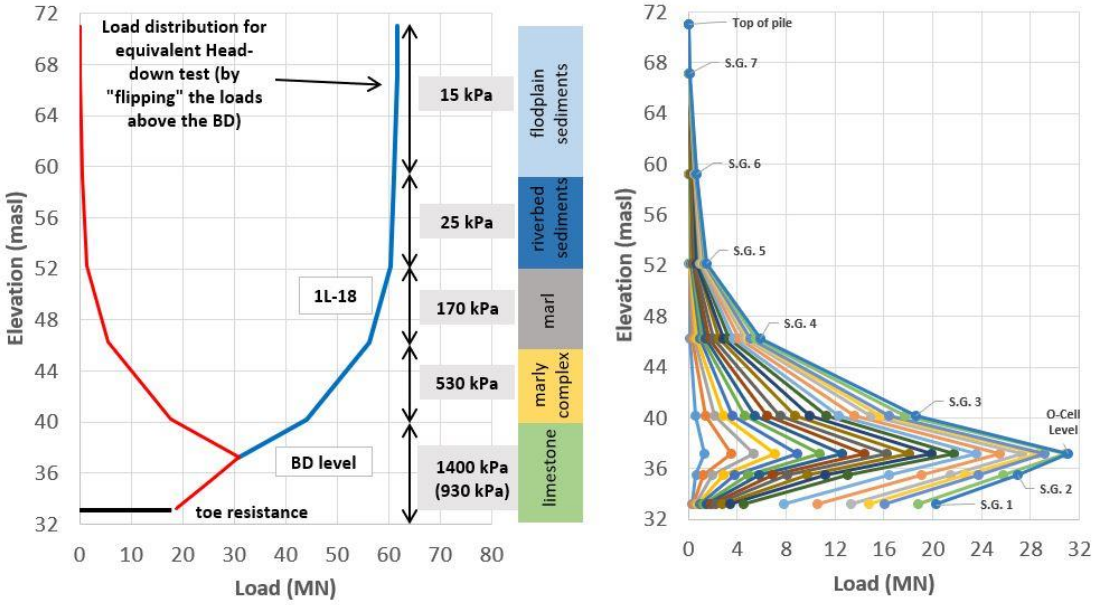

Figure 15. TP-4 pile setup with load distribution.

There are several frequently used direct CPT methods for calculating axial pile capacity. In recent years, the UniCone method [70,71] and the modified UniCone method [72], which employ all three piezocone readings (q_t, f_s and u_2), are widely used. Evaluation of unit shaft and toe resistance from the UniCone method relies on effective cone resistance $q_E = q_t - u_2$ and soil type estimation from piezocone measurements. The researchers in [71] noticed that very large u_2 values can result in unrealistically low calculated pile resistances. Marl at plot 19 is a typical representative of a soil where the UniCone method is not applicable due to high shear-induced penetration pore pressures (see Figure 7). For the soil with significant microstructure, recognized by the mismatch in soil type determination from Q_{tn}–F_r and Q–U_2 charts, q_t should be used instead of q_E for pile resistance calculation. Among the most used European methods for pile resistance calculation is the LCPC method [73].

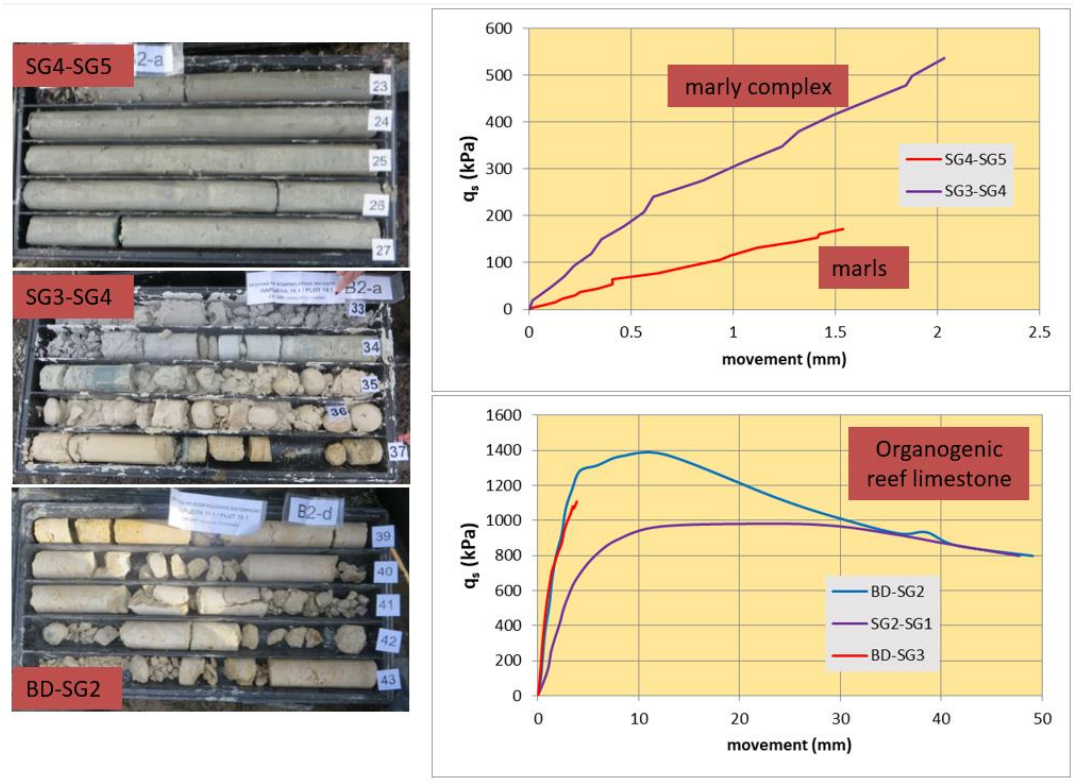

Figure 16. Mobilized shaft friction with borehole core photographs for depths within the load measurement intervals indicated in the figure.

A great experience is accumulated using the LCPC method, making it appealing to geotechnical engineers even if it uses uncorrected cone resistance (q_c) for the pore pressures acting on the cone shoulder. This method was updated in 2012 [74] to implement a larger database of full-scale tests. The application of the LCPC method relies on the proper determination of shaft and toe coefficients used to calculate unit toe resistance and shaft friction. These coefficients depend on the soil type, which is determined automatically from SBT charts [65] implemented in commercial software. If the soil type is misidentified by the SBT chart, then the shaft and toe coefficients are wrongly determined. Soils with microstructure are typical representatives of a soil where shaft and toe coefficients would be wrongly determined if one relies solely on Q_{tn}–F_r charts for the determination of soil type. By referring to Figure 7, it can be observed that marls at plot 19 are wrongly classified on the SBT chart as sandy soil (SBT groups 5 and 6). The coefficient α_{LCPC} used to calculate q_s from cone resistance proposed by the LCPC method for sandy soil is $\alpha_{LCPC} = 100$. Commercial software uses this value for automatic calculation of pile axial capacity. However, the value that should be used based on a soil description is $\alpha_{LCPC} = 60$. This yields a relative error in calculated shaft friction of 40%. Table 3 compares shaft friction obtained from LCPC method using different values for α_{LCPC}.

The coefficient α_{LCPC} is adopted for soil type determined by the SBT chart [65] and field/laboratory description. Results indicate that LCPC-calculated q_s is significantly underestimated if α_{LCPC} is determined from the SBT soil type chart. This finding also applies to other methods that rely on the SBT index for soil classification. For cases where α_{LCPC} is adopted for the soil type determined by field observations, shaft friction is more precisely predicted. All calculations performed

adopt a value of q_c = 8.5 MPa (average value from 22 m to 26 m depth). Both LCPC methods give similar q_s. However, larger q_c yields larger differences in calculated q_s, with higher values obtained by the original LCPC method. [75] reported that the LCPC 2012 method has the best statistic in terms of shaft friction prediction. As shown in Table 3, the LCPC 2012 method yields slightly lower values of q_s compared to the original method. In a similar manner, six MPT results were used to calculate q_s from p^*_{LM} using the [74] method described by [76].

Table 3. Calculated and measured shaft friction in marls.

Equation for q_s	q_s in kPa	q_s* in kPa (measured)
q_c/α_{LCPC}, α_{LCPC}=100 (SBT)	85	170
q_c/α_{LCPC}, α_{LCPC}=60 (field)	139	
$k \cdot g_i(q_c)$, k=1.4 for marl	142	
$k \cdot g_i(p^*_{LM})$, k=1.5 for marl	143-186 (162)	

Note: Parameter k depends on pile type and installation method. Functions $g_i(q_c)$ and $g_i(p^*_{lM})$ depend on soil type. More details about k and g_i can be found in [76]; *q_s not fully mobilised (see figure 16, SG4-SG5 curve).

The results of these calculations are shown in Table 3, including minimal, maximal, and average values of q_s. It can be seen that the MPT method is the most reliable method compared to the LCPC methods. However, the reference measured unit shaft friction was not fully mobilized in the BD static load test.

6. Conclusions

In this paper, we show soil characterization using three common in situ tests: CPT, SDMT, and MPT. A full-scale BD static load test is performed for design recommendations validation and establishment of unit shaft friction and end bearing for further design purposes. The test shows that full shaft friction in limestone is mobilized at 0.01·D (12 mm), which is a frequently observed value during static load testing. Organogenic reef limestone shows strain-softening behavior during loading. This behavior can be modeled using appropriate load-transfer curves, and design values of q_s should consider allowable movements of the structure. For other parts of the pile, shaft friction is only partially mobilized. For this study, marls are the most significant geotechnical unit since they are one of the most common units in the zone of influence for structures in the Old Belgrade area. Calculated values of q_s in marls underestimate shaft bearing capacity. Among several methods, the most reliable prediction is obtained using the MPT 2012 method. It is important to mention that in soils with significant microstructure (like marls), automatic calculation of pile axial capacity using commercial software can give misleading results due to poor determination of soil type and wrong selection of coefficients used to calculate unit shaft and base resistances.

By comparing Q_{tn}–F_r and Q–U_2 charts given in Figures 6 and 7, it can be concluded that marls at plot 19 are significantly different compared to marls at plot 12. This may be attributed to the higher overconsolidation of marls at plot 19. It is not uncommon that the thickness of eroded overburden varies significantly even in a relatively small area such as BW. Reliable geological evidence that

supports this conclusion is [77]. Based on analysis of test results, marls at plot 19 can be considered as intermediate soil, or a transition from hard soil to soft rock, representing the upper limit for application of direct push in CPT or DMT tests and pre-bored MPT.

At plot 12, the situation is more favorable in terms of using the soil-oriented tests mentioned previously. It was found that in order to fit laboratory OCR/YSR, the exponent m in Eq. 4 should be varied depending on the soil type. Values of m that best fit laboratory data are indicated in Figure 8. In our situation, SDMT standard correlations slightly better predict soil parameters (OCR and M) compared to CPT correlations. The choice of appropriate CPT correlations used to derive parameters should be determined from local experience by comparison to reliable reference data.

Author contributions

Dušan Berisavljević: Writing–draft manuscript: Methodology; Graphical representation; Software; Conceptualization; Data base; Zoran Berisavljević: Writing–review and editing; Conceptualization.

Use of AI tools declaration

The authors declare they have not used Artificial Intelligence (AI) tools in the creation of this article.

Conflict of interest

The authors declare no conflict of interest.

References

1. L'Heureux JS, Lunne T (2020) Characterization and engineering properties of natural soils used for geotesting. *AIMS Geosci* 6: 35–53. https://doi.org/10.3934/geosci.2020004
2. Paniagua P, D'Ignazio M, L'Heureux JS, et al. (2019) CPTU correlations for Norwegian clays: an update. *AIMS Geosci* 5: 82–103. https://doi.org/10.3934/geosci.2019.2.82
3. Mayne PW, Cargill E, Miller B (2019) Geotechnical characteristics of sensitive Leda clay at Canada test site in Gloucester, Ontario. *AIMS Geosci* 5: 390–411. https://doi.org/10.3934/geosci.2019.3.390
4. Di Buò B, D'Ignazio M, Selänpää J, et al. (2019) Investigation and geotechnical characterization of Perniö clay, Finland. *AIMS Geosci* 5: 591–616. https://doi.org/10.3934/geosci.2019.3.591
5. Gundersen AS, Hansen RC, Lunne T, et al. (2019) Characterization and engineering properties of the NGTS Onsøy soft clay site. *AIMS Geosci* 5: 665–703. https://doi.org/10.3934/geosci.2019.3.665
6. Blaker Ø, Carroll R, Paniagua P, et al. (2019) Halden research site: geotechnical characterization of a post glacial silt. *AIMS Geosci* 5: 184–234. https://doi.org/10.3934/geosci.2019.2.184

7. Bihs A, Long M, Nordal S (2020) Geotechnical characterization of Halsen-Stjørdal silt, Norway. *AIMS Geosci* 6: 355–377. https://doi.org/10.3934/geosci.2020020
8. Igoe D, Gavin K (2019) Characterization of the Blessington sand geotechnical test site. *AIMS Geosci* 5: 145–162. https://doi.org/10.3934/geosci.2019.2.145
9. Quinteros S, Gundersen A, L'Heureux JS, et al. (2019) Øysand research site: Geotechnical characterisation of deltaic sandy-silty soils. *AIMS Geosci* 5: 750–783. https://doi.org/10.3934/geosci.2019.4.750
10. Tonni L, Gottard G (2019) Assessing compressibility characteristics of silty soils from CPTU: lessons learnt from the Treporti Test Site, Venetian Lagoon (Italy). *AIMS Geosci* 5: 117–144. https://doi.org/10.3934/geosci.2019.2.117
11. Vuksanović MZ (2015) Bara Venecija and Savamala: The railway and the city. *Nasleđe* 16: 9–26. https://doi.org/10.5937/nasledje1516009V
12. Momirov Đ, Ristić-Vakanjac V, Polomčić D, et al. (2022) Contribution to the knowledge of the ground water regime of the left bank of Sava river on the stretch Obrenovac-Belgrade. XVII Serbian symposium on hydrogeology. 395–400. Available from: http://dr.rgf.bg.ac.rs/s/repo/item/0007184.
13. CEN, 7: Geotechnical design—Part 2: Ground investigation and testing. European Committee for Standardization. 2007.
14. Ladd CC, DeGroot DJ (2003) Recommended practice for softground site characterization. *Proceedings of the 12th Pan American conference on soil mechanics and geotech-nical engineering*, Boston. Available from: https://www.geoengineer.org/index.php/publications/online-library?keywords=D.J.%20DeGroot.
15. Technical documentation—Plot 32 residential. Design brief. Available from: Author's database.
16. Berisavljević D, Filipović V, Stanisavljević N, et al. (2018) Experimental analysis of bi-directional pile static load test. *XVI Danube—European Conference on Geotechnical Engineering*, Skopje, R. Macedonia.
17. Berisavljević D, Žugić Ž, Filipović V, et al. (2019) Bi-directional (BD) static load test of bored pile socketed into limestone—lessons learned. *ISRM Specialized conference Geotechnical challenges in Karst*, Omiš, Split, Croatia.
18. Berisavljević D, Berisavljević Z (2020) Dilatometer and seismic dilatometer tests in different depositional environments. *6th International Conference on Geotechnical and Geophysical Site Characterization*. Budampest.
19. Delage P (2010) A microstructure approach to the sensitivity and compressibility of some Eastern Canada sensitive clays. *Geotechnique* 60: 353–368. https://doi.org/10.1680/geot.2010.60.5.353
20. Delage P, Lefebvre G (1984) Study of the structure of a sensitive Champlain clay and of its evolution during consolidation. *Can Geotech J* 21: 21–35. https://doi.org/10.1139/t84-003
21. Robertson PK, Kabal K (2024) *Guide to Cone Penetration Testing*, 7th Edition. Available from: https://www.cpt-robertson.com.
22. Skemptom AW (1953) The Colloidal "Activity" of Clays. *Proceedings of the 3rd International Conference of Soil Mechanics and Foundation Engineering*, 57–60.
23. ISO 22476-1: 2022 Geotechnical investigation and testing—Field testing. Part 1: Electrical cone and piezocone penetration test. 2022. Available from: https://www.iso.org/standard/75661.html.

24. ISO 22476-4, Geotechnical investigation and testing—Field testing. Part 4: Prebored pressuremeter test by Ménard procedure. 2021. Available from: https://www.iso.org/standard/75662.html.
25. ISO 22476-11, Geotechnical investigation and testing—Field testing. Part 11: Flat dilatometer test. 2017. Available from: https://www.iso.org/standard/66434.html.
26. ASTM D7400/D7400M-19 Standard Test Methods for Downhole Seismic Testing. 2019. Available from: https://store.astm.org/d7400_d7400m-19.html.
27. ASTM D1143/D1143M-20 Standard Test Methods for Deep Foundation Elements Under Static Axial Compressive Load. 2024. Available from: https://store.astm.org/d1143_d1143m-20.html.
28. Robertson PK (2009) Interpretation of cone penetration tests—a unified approach. *Can Geotech J* 46: 1337–1355. https://doi.org/10.1139/T09-065
29. Robertson PK (2012) The James K Mitchell Lecture: Interpretation of in-situ tests—some insights. *Proceedings 4th International Conference on Geotechnical and Geophysical Site Characterization–ISC*, Recife, Brazil.
30. Mayne PW (2014) Interpretation of geotechnical parameters from seismic piezocone tests. *Proceedings 3rd International Symposium on Cone Penetration Testing*, 47–73.
31. Kulhawy FH, Mayne PW (1990) Manual on Estimating Soil Properties for Foundation Design. Electric Power Research Institute, Palo Alto, 306.
32. Mayne PW (2007) In-situ test calibrations for evaluating soil parameters. *Characterization and Engineering Properties of Natural Soils*, 3. https://doi.org/10.1201/NOE0415426916.CH2
33. Schneider JA, Moss RES (2011) Linking cyclic stress and cyclic strain based methods for assessment of cyclic liquefaction triggering in sands. *Geotechnique Lett* 1: 31–36. https://doi.org/10.1680/geolett.11.00021
34. Mayne PW (2016) Evaluating effective stress parameters and undrained shear strengths of soft-firm clays from CPT and DMT. *Aust Geomech J* 51: 27–55.
35. Marchetti S, Monaco P, Totani G, et al. (2001) The flat dilatometer (DMT) in soil investigations (ISSMGE TC16). *Proceedings International Conference on In-Situ Measurement of Soil Properties and Case Histories*, Bali, Indonesia, 95–131.
36. Mair RJ, Wood DM (2013) *Pressuremeter Testing—Methods and Interpretation*, Elsevier.
37. Marsland A, Randolph MF (1977) Comparisons of the results from pressuremeter tests and large insitu plate tests in London Clay. *Geotechnique* 27: 217–243. https://doi.org/10.1680/geot.1977.27.2.217
38. Whittle AJ, Aubeny CP, Rafalovich A, et al. (1990) Interpretation of in-situ testing of cohesive soils using rational methods.
39. Chung S, Randolph M, Schneider J (2006) Effect of Penetration Rate on Penetrometer Resistance in Clay. *J Geotech Geoenviron Eng* 132. https://doi.org/10.1061/(ASCE)1090-0241(2006)132:9(1188)
40. Finno RJ (1993) Analytical interpretation of dilatometer penetration through saturated cohesive soils. *Geotechnique* 43: 241–254. https://doi.org/10.1680/geot.1993.43.2.241
41. Yu HS (2006) The First James K. Mitchell Lecture In situ soil testing: from mechanics to interpretation. *Geomech Geoeng* 1: 165–195. https://doi.org/10.1080/17486020600986884

42. Martinez A, Chen Y, Anilkumar R (2024) Bio-inspired site characterization - towards soundings with lightweight equipment. 7*th International Conference on Geotechnical and Geophysical Site Characterization*, Barcelona, Spain. https://www.scipedia.com/sj/isc2024
43. Hunt OM, O'Hara KB, Chen Y, et al. (2023) Numerical and Physical Modeling of the Effect of the Cone Apex Angle on the Penetration Resistance in Coarse-Grained Soils. *Int J Geomech* 23: 04022273. https://doi.org/10.1061/(ASCE)GM.1943-5622.0002626
44. Borela R, Frost JD, Viggiani G, et al. (2021) Earthworm-Inspired Robotic Locomotion in Sand: An Experimental Study Using X-Ray Tomography. *Géotechnique Lett* 11: 66–73. https://doi.org/10.1680/jgele.20.00085
45. Kim K, Prezzi M, Salgado R, et al. (2008) Effect of Penetration Rate on Cone Penetration Resistance in Saturated Clayey Soils. *J Geotech Geoenviron Eng* 134: 1142–1153. https://doi.org/10.1061/(ASCE)1090-0241(2008)134:8(1142)
46. Jaeger RA, Dejong JT, Boulanger RW, et al. (2010) Variable penetration rate CPT in an intermediate soil. *Proceedings of the 2nd International Symposium on Cone Penetrometer Testing*, Huntington Beach, CA.
47. Marchetti S (2015) Some 2015 Updates to the TC16 DMT Report 2001. *The 3rd International Conference on the Flat Dilatometer*, Rome, 43–65.
48. Schnaid F, Odebrecht E (2015) Challenges in the interpretation of the DMT in tailings. *The 3rd International Conference on the Flat Dilatometer DMT-15*, Rome, 13–24.
49. Dientmann G, Schnaid F, Maghous S, et al. (2018) Piezocone Penetration Rate Effects in Transient Gold Tailings. *J Geotech Geoenviron Eng* 144. https://doi.org/10.1061/(ASCE)GT.1943-5606.0001822
50. Schnaid F, Odebrecht E, Sosnoski J, et al. (2016) Effects of test procedure on flat dilatometer test (DMT) results in intermediate soils. *Can Geotech J* 53: 1270–1280. https://doi.org/10.1139/cgj-2015-0463
51. Robertson PK (2016) Cone penetration test (CPT)-based soil behavior type (SBT) classification system—an update. *Can Geotech J* 53: 1910–1927. https://doi.org/10.1139/cgj-2016-0044
52. Berisavljević D, Berisavljević Z (2019) Determination of the presence of microstructure in a soil using a seismic dilatometer. *Bull Eng Geol Environ* 78: 1709–1725. https://doi.org/10.1007/s10064-018-1234-5
53. Berisavljević D, Berisavljević Z, Čebašek V, et al. (2014) Characterisation of collapsing loess by seismic dilatometer. *Eng Geol* 181: 180–189. https://doi.org/10.1016/j.enggeo.2014.07.011
54. Marchetti S, Monaco P, Totani G, et al. (2008) In situ tests by seismic dilatometer (SDMT). In: Laier JE, Crapps DK, Hussein MH, Eds., *From Research to Practice in Geotechnical Engineering*, 292–311. https://doi.org/10.1061/40962(325)7
55. Long M (2022) Practical use of shear wave velocity measurements from SCPTU in clays—key note lecture. *5th International Symposium on Cone Penetration Testing (CPT'22)*, Bologna, Italy, CRC Press/Balkema, Leiden, the Netherlands, 28–54.
56. Berisavljević D, Božović N, and Stanić N (2024) Paired in situ tests for site characterization and geotechnical design optimization. *Proceedings of the 7th International Conference on Geotechnical and Geophysical Site Characterization Barcelona.*

57. Robertson PK (2015) Soil behavior type using the DMT. *Proceedings of the 3rd International Conference on the Flat Dilatometer DMT'15*, Roma, 243–250.
58. Berisavljević D (2017) Geotechnical soil modeling based on parameters obtained by seismic dilatometer test. Doctoral dissertation. Faculty of Mining and Geology, University of Belgrade, Belgrade, 208. https://nardus.mpn.gov.rs/handle/123456789/9155
59. Schneider JA, Randolph MF, Mayne PW, et al. (2008) Analysis of factors influencing soil classification using normalized piezocone tip resistance and pore pressure parameters. *J Geotech Geoenviron Eng* 134: 1569–1586. https://doi.org/10.1061/(ASCE)1090-0241(2008)134:11(1569)
60. Mayne PW, Coop MR, Springman S, et al. (2009) State-of-the-Art Paper (SOA-1): Geomaterial Behavior and Testing. *Proceedings of the 17th International Conference on Soil Mechanics & Geotechnical Engineering*, Millpress/IOS Press Rotterdam, 2777–2872.
61. Maraš-Dragojević S (2012) Ground surface settlement induced by tunneling. Doctoral dissertation. Faculty of Civil engineering, University of Belgrade.
62. Rinaldi VA, Santamarina JC, Redolfi ER (1998) Characterization of collapsible soils with combined geophysical and penetration testing. *Proceedings of the First International Conference on Site Characterization*, ISC'98, Atlanta, Georgia.
63. Fernandez A, Santamarina JC (2001) Effect of cementation on the small strain parameters of sands. *Can Geotech J* 38: 191–199. https://doi.org/10.1139/t00-081
64. Marchetti S (1980) In situ tests by flat dilatometer. *J Geotech Eng* 106: 299–321. https://doi.org/10.1061/AJGEB6.0000934
65. Robertson PK (1990) Soil classification using the cone penetration test. *Can Geotech J* 27: 151–158. https://doi.org/10.1139/t90-014
66. Monaco P, Totani G, Calabrese M (2006) DMT predicted vs observed settlements: a review of the available experience. *Proceedings 2nd International Conference on the Flat Dilatometer*, Washington D.C., 244–252.
67. Amar S (1991) International Society of Soil Mechanics and Foundation Engineering European Technical Committee on Pressuremeters, The Application of Pressuremeter Test Results to Foundation Design in Europe: A State-of-the-Art Report by the ISSMFE European Technical Committee on Pressuremeters. Part 1, Predrilled Pressuremeters and Self-Boring Pressuremeters. Rotterdam: A.A. Balkema. Available from: https://search.worldcat.org/title/973237426
68. Clark BG (2023) *Pressuremeters in geotechnical design*, 2nd edition. London, UK. CRC press. https://doi.org/10.1201/9781003028925
69. Baud JP, Gambin M (2014) Soil and Rock classification from high pressure borehole expansion tests. *Geotech Geol Eng* 32: 1397–1403. https://doi.org/10.1007/s10706-014-9752-9
70. Eslami A, Fellenius BH (1997) Pile capacity by direct CPT and CPTu methods applied to 102 case histories. *Can Geotech J* 34: 886–904. https://doi.org/10.1139/t97-056
71. Fellenius BH (2023) *Basics of foundation design*, Electronic Edition, 546.
72. Niazi F, Mayne P (2016) CPTu-based enhanced UniCone method for pile capacity. *Eng Geol* 212: 21–34. https://doi.org/10.1016/j.enggeo.2016.07.010
73. Bustamante M, Gianeselli L (1982) Pile bearing capacity predictions by means of static penetrometer CPT. *Proceedings of the 2nd European Symposium on Penetration Testing*, ESOPT II, Amsterdam, A.A. Balkema, Rotterdam, 2: 493–500.

74. AFNOR, Calcul des fondations profondes—NF P 94 262. French standard, 2012. In French. Available from: https://www.boutique.afnor.org/en-gb/standard/nf-p94262/justification-of-geotechnical-work-national-application-standards-for-the-i/fa152485/39475.
75. Doan LV, Lehane BM (2021) CPT-Based Design Method for Axial Capacities of Drilled Shafts and Auger Cast-in-Place Piles. *J Geotech Geoenviron Eng* 147. https://doi.org/10.1061/(ASCE)GT.1943-5606.0002542
76. Burlon S, Frank R, Baguelin F, et al. (2014) Model factor for the bearing capacity of piles from pressuremeter test results—Eurocode 7 approach. *Géotechnique* 64: 513–525. http://dx.doi.org/10.1680/geot.13.P.061
77. Rundić L, Ganić M, Knežević S, et al. (2010) Upper Miocene Pannonian sediments from Belgrade (Serbia): new evidence and paleoenvironmental considerations. *Geologica Carpatica* 62: 267—278.